Widespread male-female expression imbalance of X-linked genes across phrynosomatid lizards

Matthew D. Hale[1,2,*], Pietro L. H. de Mello[1], Daniel T. Nondorf[1], Christopher D. Robinson[1,3], Henry B. John-Alder[4], Christian L. Cox[5], and Robert M. Cox[1,*]

[1] Department of Biology, University of Virginia, Charlottesville, VA 22904

[2] U.S. Military HIV Research Program, Walter Reed Army Institute of Research, Silver Spring, MD 20910; Henry M. Jackson Foundation for the Advancement of Military Medicine, Inc., Bethesda, MD, 20817

[3] School of Life Sciences, Arizona State University, Tempe, AZ 85287

[4] Department of Ecology, Evolution, and Natural Resources, Rutgers University, New Brunswick, NJ 08901

[5] Department of Biological Sciences, Florida International University, Miami, FL 33199

Authors for Correspondence:

*Matthew D. Hale: U.S. Military HIV Research Program, Walter Reed Army Institute of Research, Silver Spring, MD 20910, USA; Henry M. Jackson Foundation for the Advancement of Military Medicine, Inc., Bethesda, MD, 20817, USA. Phone: 301-319-3082. Email: mhale@hivresearch.org

*Robert M. Cox: Department of Biology, University of Virginia, Charlottesville, VA, 22904, USA. Phone: 434-982-1987. Email: rmc3u@virginia.edu

Abstract

Classic theory on sex chromosome evolution predicts that selection should restore ancestral diploid expression for hemizygous X-linked genes in males. However, this dosage compensation is often incomplete, leaving X enriched for genes with female-biased expression. In this context, iguanian lizards are noteworthy among vertebrates because several species from separate families appear to exhibit both near-complete dosage compensation and male-female expression balance across their ancient, homologous X chromosomes. We tested for this pattern in the phrynosomatid *Sceloporus undulatus* (Eastern Fence Lizard) and instead found that both ancient and more recently sex-linked regions of the X chromosome are enriched for genes with female-biased expression, regardless of age (neonate, juvenile, adult) or tissue (brain, liver, muscle). By expanding our analysis across 10 phrynosomatid species spanning 4 genera, we found that male-female expression imbalance on the ancestral region of X is phylogenetically conserved. We also found that an inferred chromosomal rearrangement in the *S. jarrovii* lineage has resulted in the novel acquisition of female-biased expression by a region of formerly autosomal genes. Whereas sex-biased expression of the ancestral region of X is primarily due to females overexpressing X-linked genes relative to autosomal genes, sex-biased expression of these formerly autosomal genes in *S. jarrovii* is primarily due to males underexpressing this putative neo-X region. We conclude that male-female expression imbalance on X is widespread across phrynosomatids, potentially reflecting both overexpression in females for ancestral regions that have evolved dosage compensation and underexpression in males for neo-X regions in which dosage compensation has yet to evolve.

Keywords: autosome, dosage compensation, sex-biased gene expression, sex chromosome, transcriptome

Introduction

The evolution of sex chromosomes poses a recurring challenge because sex-limited Y or W chromosomes typically degenerate due to the suppression of recombination with formerly homologous X or Z chromosomes, resulting in the loss of functional gene content on Y or W (Charlesworth 2021; Graves 2016; Saunders and Muyle 2024). Consequently, genes on X or Z become hemizygous in the heterogametic sex, potentially disrupting protein stoichiometry with autosomal gene products and thus eliciting negative effects on cell function and organismal fitness (Bachtrog et al. 2011; Birchler et al. 2005; Mank 2009; Shaw and White 2022; Veitia and Potier 2015). Classic theory by Ohno (1967) predicts that this deleterious hemizygous state should favor the evolution of compensatory mechanisms that restore ancestral levels of expression for X- or Z-linked genes in the heterogametic sex (Graves 2016; Gu and Walters 2017). Although such dosage compensation has evolved in many taxa, sex chromosomes are nonetheless often enriched for genes with sex-biased expression (Albritton et al. 2014; Chen et al. 2020a; Furman et al. 2020). This enrichment could indicate that sex chromosomes are hotspots for genes with sexually antagonistic fitness effects (Allen et al. 2013; Dean and Mank 2014). However, it is primarily thought to occur because dosage compensation is incomplete and evolves on a gene-by-gene basis (Chen et al. 2020a; Darolti et al. 2019; Furman et al. 2020; Gu and Walters 2017; Mank 2013, 2009; Mullon et al. 2015), or because dosage compensation in the heterogametic sex results in the overexpression of X or Z in the homogametic sex (Allen et al. 2013; Bista et al. 2021; Mank et al. 2011; Prince et al. 2010; Wright and Mank 2012). This underscores a key distinction between "sex-chromosome dosage compensation" (*i.e.,* equal expression of X or Z relative to autosomes in the heterogametic sex) and "male-female expression balance" (*i.e.,* equal expression of X or Z in the heterogametic sex relative to X or Z

72 in the homogametic sex) as two separate phenomena (Bista et al. 2021; Disteche 2012; Gu and
73 Walters 2017; Mank 2009).
74 Although some species exhibit both dosage compensation and male-female expression
75 balance (Lucchesi and Kuroda 2015; Metzger et al. 2021; Vicoso and Bachtrog 2015), others
76 appear to lack dosage compensation despite male-female balance (Albritton et al. 2014; Gu et al.
77 2017; Pessia et al. 2014), lack male-female balance despite dosage compensation (Allen et al.
78 2013; Muyle et al. 2018; Prince et al. 2010; Schultheiß et al. 2015), or lack both dosage
79 compensation and male-female balance (Chen et al. 2014; Itoh et al. 2010; Mank 2013).
80 Therefore, many exceptions to Ohno's (1967) pioneering theory of dosage compensation have
81 emerged, and complete dosage compensation across the entire X or Z chromosome is now
82 considered the exception rather than the rule (Chandler 2017; Chen et al. 2020a; Furman et al.
83 2020; Gu and Walters 2017; Mank 2022, 2013, 2009). Overall, dosage compensation appears to
84 be more common in XY than in ZW systems, but the generality of this trend varies across
85 lineages and its potential underlying causes are unclear (Gu and Walters 2017; Mank 2013;
86 Mullon et al. 2015; Vicoso et al. 2013b). One limitation of our current understanding of dosage
87 compensation and male-female expression balance is that it is derived from a relatively limited
88 diversity of taxa (Chen et al. 2020a; Gu and Walters 2017; Kratochvil et al. 2021; Saunders and
89 Muyle 2024). To help address this limitation, we tested for dosage compensation and male-
90 female expression balance across a large reptile lineage with ancestral XY sex-determination.
91 Squamate reptiles (lizards and snakes) are a promising group for studies of dosage
92 compensation because they have repeatedly evolved both XY and ZW sex determination, vary
93 widely in the extent of sex chromosome degeneration and heteromorphism, and exhibit frequent
94 rearrangements between sex chromosomes and autosomes (Alam et al. 2018; Deakin and Ezaz

95 2019; Gamble et al. 2015; Giovannotti et al. 2017; Leaché et al. 2016; Lisachov et al. 2021;
96 Pennell et al. 2015). Yet, dosage compensation and male-female expression balance have only
97 been characterized in a few squamate reptiles, primarily due to the historical lack of high-quality
98 genome assemblies (Pinto et al. 2023). Dosage compensation is partial in the viperid rattlesnakes
99 *Crotalus viridis* and *Sistrurus miliarius*, in which Z also lacks male-female expression balance
100 (Schield et al. 2019; Vicoso et al. 2013a). Z also lacks both male-female expression balance and
101 dosage compensation in the varanid lizard *Varanus komodoensis* and the related helodermatid
102 lizard *Heloderma suspectum*, which have homologous Z chromosomes (Rovatsos et al. 2019;
103 Webster et al. 2024). By contrast, the anolid lizard *Anolis carolinensis* is one of the few
104 vertebrates to exhibit near-complete dosage compensation and male-female expression balance
105 on its X chromosome (Chen et al. 2020a; Marin et al. 2017; Rovatsos and Kratochvíl 2021; Rupp
106 et al. 2017). While this appears to support the generalization that dosage compensation is more
107 common in XY than in ZW systems, the corytophanid lizard *Basiliscus vittatus* and the
108 pygopodid lizard *Lialis burtonis* have each evolved different XY systems that lack male-female
109 expression balance on X (Acosta et al. 2019; Nielsen et al. 2019; Rovatsos et al. 2021).
110 Interestingly, recent data from the phrynosomatid lizard *Urosaurus nigricaudus,* which
111 has an ancient X chromosome homologous to that of *Anolis carolinensis*, suggest the presence of
112 both dosage compensation and male-female expression balance on X (Davalos-Dehullu et al.
113 2023). This raises the question of whether the dosage compensation and male-female expression
114 balance observed in *Anolis carolinensis,* which involves an epigenetic mechanism for male-
115 specific upregulation of X that is reminiscent of that found in *Drosophila* (Marin et al. 2017), is
116 conserved across phrynosomatids and other iguanian lineages that share a homologous X
117 chromosome. We addressed this question by characterizing gene expression in the Eastern Fence

118 Lizard (*Sceloporus undulatus*) and nine related species spanning four genera in the family
119 Phrynosomatidae, one of twelve families in the large (>1,250 species) Pleurodonta clade of
120 iguanian lizards. With the exception of corytophanids, all families in Pleurodonta (including the
121 genera *Anolis, Sceloporus,* and *Urosaurus* mentioned above) share an ancestral XY system that
122 arose over 100 Mya and is thus comparable in age to the ancient eutherian and monotreme XY
123 systems and the avian and ophidian ZW systems (Acosta et al. 2019; Altmanova et al. 2018;
124 Davalos-Dehullu et al. 2023; Marin et al. 2017; Nielsen et al. 2019; Rovatsos et al. 2014b).
125 Regions of this ancient iguanian X chromosome exhibit broad synteny across several anolid and
126 phrynosomatid genomes (Davalos-Dehullu et al. 2023; Geneva et al. 2022; Westfall et al. 2021)
127 and hemizygosity in males of several anolid and phrynosomatid species (Geneva et al. 2022;
128 Rovatsos et al. 2014a), as well as both dosage compensation and male-female expression balance
129 in *A. carolinensis* (Chen et al. 2020a; Marin et al. 2017) and potentially also in phrynosomatids
130 such as *Urosaurus nigricaudus* and *U. bicarinatus* (Davalos-Dehullu et al. 2023).
131 In this study, we assessed synteny of the X chromosome between *Sceloporus undulatus*
132 and other iguanian genomes, then quantified sex-specific DNA dosage along the *S. undulatus* X
133 chromosome to identify regions of male hemizygosity. Using transcriptomic data from multiple
134 ages and tissues, we identified genes that are consistently sex-biased in their expression in *S.*
135 *undulatus*, determined their chromosomal locations, and tested for both sex-chromosome dosage
136 compensation and male-female expression balance. We conducted these tests separately for the
137 ancestral region of X that is hemizygous in males and for a small neo-X region in *S. undulatus*
138 that maps to autosomes in several other phrynosomatids and in *A. carolinensis*. While replicating
139 these tests in a congener, we uncovered the transcriptomic signature of another neo-X region in
140 *S. jarrovii*, which we also tested for dosage compensation and male-female expression balance.

141 Using liver transcriptomes from seven *Sceloporus* species and three representatives of other
142 phrynosomatid genera, we characterized broad evolutionary trends in sex-biased gene expression
143 across the putatively homologous region of their ancient iguanian X chromosome, as well as the
144 two neo-X regions identified within *S. undulatus* and *S. jarrovii*. Collectively, these analyses
145 extend our understanding of dosage compensation in squamate reptiles, reveal that male-female
146 expression imbalance is widespread across phrynosomatid lizards, and suggest that male-female
147 expression imbalance can occur in the presence of dosage compensation for ancient X-linked
148 genes, or in the absence of dosage compensation for more recently X-linked genes.
149

150 **Results**

151 The X Chromosome of *S. undulatus* has an Ancient Hemizygous Region and a Neo-X Region

152 Westfall et al. (2021) identified the tenth largest scaffold in the *S. undulatus* assembly
153 (NC_056531.1, 16.86 Mbp, hereafter chromosome 10) as the predicted X chromosome. Our
154 analyses confirm that the majority (15.10 Mbp) of *S. undulatus* chromosome 10 is syntenic with
155 the ancient X chromosome in other iguanian genomes, including the more distantly related
156 anolids *Anolis carolinensis* and *A. sagrei* and the more closely related phrynosomatids
157 *Phrynosoma platyrhinos* and *Urosaurus ornatus* (Fig. 1), which agrees with another recent
158 synteny analysis (Davalos-Dehullu et al. 2023). However, we also found that a small (1.76 Mbp),
159 distal region of *S. undulatus* chromosome 10 is syntenic with a portion of a putatively autosomal
160 microchromosome in *Phrynosoma platyrhinos* (Fig. 1A), suggesting that this is a more recently
161 X-linked region in *S. undulatus*. Targeted BLAST searches of predicted mRNA sequences from
162 this distal region confirmed that individual genes located before 15.10 Mbp on chromosome 10
163 in *S. undulatus* typically map to X in all other iguanians (Fig. 1B), whereas genes located after

164 15.10 Mbp only map to X in closely related *S. tristichus* (formerly considered a subspecies of *S.*
165 *undulatus*) and distantly related *A. sagrei* (due to an independent X-autosome fusion, (Geneva et
166 al. 2022)). In other phrynosomatids (*U. nigricaudus, P. platyrhinos*) and other distantly related
167 anolids (*A. carolinensis*), genes located after 15.10 Mbp on the *S. undulatus* X chromosome map
168 to putative autosomes or unplaced scaffolds (Fig. 1B).

169 Analysis of published whole-genome sequences from 18 female and 11 male *S. undulatus*
170 specimens (Assis et al. 2025) revealed that $\log_2$ (male/female) DNA coverage is centered at 0
171 (equal dosage) across all chromosomes except chromosome 10 (Table S2; Fig. S1), which
172 exhibits values near -1 (two-fold higher DNA coverage in females) along most of its length (Fig.
173 1C). However, chromosome 10 exhibits a distinct shift toward values centered on 0 beginning at
174 approximately 14.85 Mbp, slightly before the start of the putative neo-X region at 15.10 Mbp
175 (Fig. 1C). Whereas most genes between 14.85 and 15.10 Mbp have DNA coverage ratios near 0,
176 genes located after 15.10 Mbp exhibit a range of values between 0 and -1, suggesting that the
177 homologous neo-Y region may be in the process of degeneration (Fig. 1C). In our subsequent
178 analyses of dosage compensation (below), we excluded the 15 genes located between 14.85 and
179 15.10 Mbp of chromosome 10 because these genes are ancestrally X-linked (Fig. 1B) but exhibit
180 no evidence of a sex difference in dosage (Fig. 1C), suggesting that they may reside on an
181 ancient pseudoautosomal region (PAR) that is still recombining with the Y chromosome.

182 Although the *S. undulatus* genome was sequenced from male tissue, the current assembly
183 does not include a Y chromosome (Westfall et al. 2021). However, our analyses of unplaced
184 scaffolds revealed 45 annotated genes with mean $\log_2$ (male/female) DNA coverage values
185 greater than 0.5 (Table S2). We hypothesize that many of these scaffolds, which each contain a
186 single gene and collectively comprise only 0.2 Mbp, may correspond to Y-linked regions of the

187 S. *undulatus* genome. We also found 116 annotated genes on unplaced scaffolds with mean $\log_2$
188 (male/female) DNA coverage values less than -0.5, potentially corresponding to unassembled
189 regions of the X chromosome (Table S2). Filtering to exclude genes with low coverage (mean <
190 10 in both sexes) left 44 of these potentially Y-linked genes and 65 of these potentially X-linked
191 genes on unassembled scaffolds (Fig. S1).
192
193 <u>The X Chromosome of *S. undulatus* is a Hotspot for Consistently Sex-Biased Genes</u>
194 To characterize male-female expression imbalance in *S. undulatus* without any *a priori*
195 assumptions about genomic location, we conducted genome-wide differential gene expression
196 analyses to identify genes that are consistently sex-biased in their expression across three ages
197 (neonate, juvenile, adult) in three distinct tissues (brain, liver, muscle). We reasoned that such
198 consistency is more likely to reflect sex differences in gene dosage than in gene regulation,
199 which is likely to be both age- and tissue-specific. We detected cohorts of significantly
200 differentially expressed genes (DEGs; $P < 0.05$ after correction for false discovery rate) that are
201 consistently female-biased across all ages in the liver ($n = 30$ genes; Fig. 2A-C), brain ($n = 43$;
202 Fig. S2A-C), and muscle ($n = 10$; Fig. S3A-C). We also detected cohorts of DEGs that are
203 consistently male-biased across all ages in the liver ($n = 27$; Fig. 2A-C), brain ($n = 34$; Fig. S2A-
204 C), and muscle ($n = 18$; Fig. S3A-C). These consistently sex-biased DEGs typically exhibit the
205 same patterns of sex bias across tissues (Fig. S4A-I), and many are identified as consistently sex-
206 biased DEGs in more than one tissue (Fig. S4J-K). Consistently female-biased DEGs fall within
207 a relatively narrow range of $\log_2$ FC values corresponding to approximately 1.5 to 2-fold higher
208 expression in females, while consistently male-biased DEGs exhibit a wider range of more
209 extreme $\log_2$ FC values (Figs. S2-S5). Consistently female-biased DEGs are expressed in both

210 sexes, as expected if they are located on the X chromosome, whereas many consistently male-
211 biased DEGs are expressed at low or undetectable levels in females (Fig. S5), as expected if they
212 are located on the Y chromosome.

213 The majority (43 of 55) of the consistently female-biased DEGs we identified are located
214 on the X chromosome (Fig. 2D-F; Figs. S2-S3). The remainder (12 of 55) are located on small,
215 unplaced scaffolds, many (6 of 12) of which have $\log_2$ (male/female) DNA coverage values
216 below -0.5, suggesting that they are regions of X that were orphaned during assembly (Table S2).
217 In contrast, the majority (30 of 44) of the consistently male-biased DEGs that we identified are
218 located on small, unplaced scaffolds in the *S. undulatus* assembly (Fig. 2D-F; Figs. S2-S3), most
219 of which (22 of 30) we hypothesized to be Y-linked based on $\log_2$ (male/female) DNA coverage
220 values that are above 0.5 (Table S2) or inestimable due to the absence of reads from females
221 (*e.g.,* LOC121918292, an *RPL6*-like gene; *RPL6* is known to be Y-linked in *Anolis carolinensis*;
222 Marin et al. 2017). A subset (10 of 44) of consistently male-biased DEGs are located on the X
223 chromosome. Although this could potentially occur if some Y-linked regions co-assembled with
224 X (Westfall *et al.*, 2021)*,* all of these male-biased genes on the X chromosome exhibit $\log_2$
225 (male/female) DNA coverage values near -1 (Fig. 1C), indicating that they are hemizygous in
226 males. A few (4 of 44) consistently male-biased DEGs are located on putative autosomes (Figs.
227 2D-F; S3D-F).

228 Plotting sex-biased expression as a function of chromosomal location across the 11
229 largest scaffolds in the *S. undulatus* genome reveals a single peak of elevated sex bias on the X
230 chromosome that is evident across all ages and tissues (Fig. 2G-I; Figs. S2-S3). Consistently
231 female-biased genes are widely distributed across the entire length of the X chromosome and are
232 interspersed with many unbiased genes and several consistently male-biased genes (Fig. 2J; Fig.

233 S6). Whereas both the proximal 14.85 Mbp (ancestral X-linked region that is hemizygous in
234 males) and the distal 1.76 Mbp (hypothesized neo-X region) of the X chromosome contain
235 consistently female-biased DEGs and exhibit an overall tendency toward female-biased
236 expression (Fig. S6), the intermediate 0.25 Mbp (hypothesized ancestral PAR) exhibits virtually
237 no sex-biased expression at any age or in any tissue (Fig. S6). Genes across the X chromosome
238 collectively exhibit a significant female bias in their median expression at 2 of 3 ages in liver
239 (Fig. 2D-F), 3 of 3 ages in brain (Fig. S2D-F) and 1 of 3 ages in muscle (Fig. S3D-F), and we
240 found identical results when restricting this comparison to genes in the 14.84 Mbp, ancestrally
241 X-linked region. Each of the 4 consistently female-biased DEGs in the hypothesized neo-X
242 region exhibits a negative $\log_2$ (male/female) DNA coverage value below -0.25, suggesting that
243 their gametologs in the neo-Y region have degenerated or diverged.

244 Enrichment of the X chromosome with sex-biased genes was recapitulated when we
245 repeated our analyses of *S. undulatus* transcriptomes by mapping reads to the genome of closely
246 related *S. tristichus* (formerly *S. undulatus tristichus*), which was sequenced from female tissue
247 and therefore lacks any Y-linked sequences in its assembly (Bedoya and Leaché 2021). These
248 analyses avoid any potential mapping artifacts that could have arisen if Y-linked sequences
249 either coassembled with or prevented the assembly of X-linked sequences onto chromosome 10
250 in the *S. undulatus* assembly (Figs. S7-S8, see Supplementary Results). Moreover, we did not
251 find any consistently sex-biased DEGs on chromosome 10 of the *S. undulatus* assembly that
252 yielded highly similar BLAST hits for genes with opposite patterns of sex-biased expression,
253 which would be expected if corresponding X- and Y-linked gametologs are still expressed but
254 map to different locations (see Supplementary Results). We found three examples of consistently
255 female-biased DEGs on unplaced scaffolds with BLAST hits corresponding to highly male-

256 biased DEGs on other unplaced scaffolds (Fig. S9). While these may indicate orphaned X- and
257 Y-linked gametolog pairs that collectively achieve balanced expression (Fig. S9), we found no
258 evidence for similar Y-gametolog compensation of X-linked genes on chromosome 10.
259
260 The X Chromosome of *S. undulatus* is Overexpressed Relative to Autosomes in Females
261 To determine whether male-female expression imbalance on the *S. undulatus* X
262 chromosome is driven by the lack of dosage compensation in males versus overcompensation in
263 females, we compared the expression of X-linked genes to the expression of autosomal genes
264 separately within each sex. We did this by randomly sampling 1000 contiguous regions of the
265 autosomal genome with the same number of expressed genes as the corresponding regions of X
266 to generate null distributions of median autosomal expression values for each sex, age, and tissue
267 (Fig. 3). In *S. undulatus* males, the median expression of ancestrally X-linked genes on the
268 proximal 14.85 Mbp region of the X chromosome is statistically indistinguishable from the
269 sampled autosomal distributions for liver and trends toward the high ends of the sampled
270 autosomal distributions for brain and muscle (Fig. 3A). In females, the median expression of
271 these same ancestrally X-linked genes trends toward the high ends of the simulated autosomal
272 distributions for liver and muscle and significantly exceeds the simulated autosomal distributions
273 for brain (Fig. 3A). We observed similar patterns for more recently X-linked genes on the distal,
274 1.76-Mbp region of the X chromosome (Fig. 3B). Collectively, these results indicate that female-
275 biased expression across the X chromosome is associated with elevated expression of X-linked
276 genes in females, rather than reduced expression of X-linked genes in males.

277 Consistently Sex-Biased Genes Identify a Putative Neo-X Region in *S. jarrovii*

278 To explore the phylogenetic conservation of patterns identified in *S. undulatus,* we also
279 tested for consistently sex-biased genes using liver transcriptomes from *S. jarrovii* that were
280 sampled at three ages (neonate, juvenile, adult). We detected 54 DEGs in *S. jarrovii* liver that are
281 consistently female-biased across all ages (Fig. 4A-C), as well as 12 DEGs that are consistently
282 male-biased across all ages (Fig. 4A-C). These consistently female-biased DEGs fall within a
283 relatively narrow range of $\log_2$ FC values that corresponds to approximately 2-fold higher
284 expression in females than in males, consistent with X-linkage, whereas most of the consistently
285 male-biased DEGs are expressed at low or undetectable levels in females, consistent with Y-
286 linkage (Fig. S10). Many (15 of 54) of the consistently female-biased DEGs in *S. jarrovii* map to
287 the X chromosome in *S. undulatus* (Fig. 4D-F), and the median expression of all genes that map
288 to the *S. undulatus* X chromosome is significantly female-biased at all ages in *S. jarrovii* (Fig.
289 4D-F). None of the consistently sex-biased genes in *S. jarrovii* map to the distal 1.76-Mbp region
290 of the *S. undulatus* X chromosome (Fig. 4J), and this region exhibts no overall female bias in its
291 expression in *S. jarrovii* (Fig. S11), as expected given that genes in this region map to autosomes
292 in all phrynosomatids other than *S. undulatus* and *S. tristichus* (Fig. 1).

293 Unlike in *S. undulatus*, most of the consistently female-biased DEGs (38 of 54) and half
294 of the consistently male-biased DEGs (6 of 12) that we detected in *S. jarrovii* transcriptomes
295 map to the sixth largest scaffold in the *S. undulatus* assembly (NC_056527.1, hereafter
296 chromosome 6), which is an autosome in *S. undulatus* (Fig. 4D-F). Moreover, all 44 of these
297 consistently sex-biased DEGs fall within a relatively small, 11-Mbp distal region of chromosome
298 6 (hereafter DR6; Fig. 4J) that exhibits a sharp peak of sex-biased expression similar to that
299 observed on the X chromosome (Fig. 4G-I). Genes on chromosome 6 that fall outside of DR6

300 exhibit no overall tendency toward sex-biased expression in either *S. jarrovii* or *S. undulatus*
301 (Fig. 5). However, the 156 genes located within DR6 are significantly female-biased in *S.*
302 *jarrovii*, even when excluding the subset of 44 consistently sex-biased DEGs that we first used to
303 identify this region (Fig. 5B). These 156 genes within DR6, including the 44 consistently sex-
304 biased DEGs from *S. jarrovii*, do not exhibit any overall sex bias in DNA coverage (Fig. S1) or
305 expression (Fig. 5B) in *S. undulatus*. Collectively, genes within DR6 exhibit expression profiles
306 similar to the X chromosome in *S. jarrovii,* but similar to autosomes in *S. undulatus* (Fig. 5).
307

308 <u>The Putative Neo-X Region in *S. jarrovii* Lacks Dosage Compensation in Males</u>

309 Similar to our analyses for *S. undulatus*, we compared the median expression of
310 putatively X-linked genes in *S. jarrovii* (*i.e.,* genes on the ancestrally X-linked 14.85-Mbp region
311 of *S. undulatus* chromosome 10 and the recently X-linked 11-Mbp DR6 region of *S. undulatus*
312 chromosome 6) to simulated null distributions of median autosomal expression in males and
313 females by randomly sampling 1000 contiguous regions of the autosomal genome with the same
314 number of expressed genes as the corresponding X-linked regions. In *S. jarrovii* males, median
315 levels of expression for genes mapping to the ancestrally X-linked region of *S. undulatus*
316 chromosome 10 fall within the simulated distributions for autosomal genes, but lower than the
317 median (Fig. S12A). In *S. jarrovii* females, median levels of expression for these same genes are
318 toward the high end of sampled distributions for autosomal genes (Fig. S12A). In both sexes of
319 *S. jarrovii*, the median expression of genes that map to DR10 in *S. undulatus* is near the center of
320 the simulated autosomal distribution (Fig. S12B), consistent with the interpretation that this neo-
321 X region in *S. undulatus* is not X-linked in *S. jarrovii.*

322 By contrast, the median expression of genes within DR6 is substantially reduced in *S.*
323 *jarrovii* males when compared to sampled null distributions for autosomal genes, although this
324 reduction is not statistically significant at any age (Fig. 6A). In *S. jarrovii* females, the median
325 expression of genes within DR6 is similar to the simulated distributions for autosomal genes at
326 all ages (Fig. 6A). In *S. undulatus*, the median expression of genes within DR6 is similar to the
327 simulated distribtions for autosomal genes in both sexes (Fig. 6A). Therefore, DR6 in *S. jarrovii*
328 exhibits the predicted transcriptomic profile for X-linked genes that lack dosage compensation in
329 males, whereas DR6 in *S. undulatus* is expressed at levels comparable to other autosomal genes
330 in both sexes. Paired, inter-species comparisons of *S. jarrovii* and *S. undulatus* homologs on DR6
331 corroborate this interpretation. Homologous genes on DR6 are expressed at comparable levels in
332 females of each species (paired *t*-tests within each age, all $P > 0.74$; Fig. 6B), but at significantly
333 lower levels in *S. jarrovii* males than in *S. undulatus* males (all $P < 0.001$; Fig. 6B).
334
335 Male-Female Expression Imbalance of the Ancestral X is Conserved Across Phrynosomatids
336 To characterize broad evolutionary trends in the expression of sex-linked genes, we
337 combined our expression data from adult livers in *S. undulatus* and *S. jarrovii* with similar RNA-
338 seq data (mapped to the *S. undulatus* genome) from adult livers in 5 other *Sceloporus* species,
339 plus representatives of 3 other phrynosomatid genera (Table S1). Across Phrynosomatidae, we
340 observed female-biased expression of genes mapping to the ancestrally X-linked 14.85-Mbp
341 region of *S. undulatus* chromosome 10, suggesting that this signature of male-female expression
342 imbalance is the ancestral state for this family (Fig. 7A). Median $\log_2$ male:female expression
343 ratios across this putatively homologous region of the X chromosome are significantly female-
344 biased in adult liver from 6 of 7 *Sceloporus* species (all species except *S. slevini*), as well as from

345 all 3 phrynosomatid species representing other genera (Fig. 7A). Moreover, each of the DEGs
346 from this ancestral region of chromosome 10 that are consistently female-biased across ages in *S.*
347 *undulatus* are nearly always also female-biased in other phrynosomatid species (Fig. 7A).
348 Likewise, the few DEGs from this ancestral region of chromosome 10 that are consistently male-
349 biased across ages in *S. undulatus* also tend to exhibit male-biased expression in other species,
350 although this conservation is somewhat weaker (Fig. 7A).
351
352 Male-Female Expression Imbalance of Neo-X Regions is Restricted to Individual Lineages
353 In contrast to the phylogenetically conserved patterns of sex-biased expression for genes
354 on the ancestrally X-linked region of *S. undulatus* chromosome 10 (Fig. 7A), only *S. undulatus*
355 exhibits female-biased expression of genes on its putative neo-X region comprising the distal
356 1.76 Mbp of chromosome 10 (DR10, Fig. 7B). Moreover, the few genes from DR10 that are
357 consistently female-biased DEGs across ages in *S. undulatus* exhibit no overall tendency for
358 female-biased expression in other species (Fig. 7B). Similarly, only *S. jarrovii* exhibits female-
359 biased expression for genes on its putative neo-X region comprising the 11-Mbp distal portion of
360 chromosome 6 in *S. undulatus* (DR6, Fig. 7C). Likewise, genes from DR6 that are consistently
361 either female- or male-biased DEGs across ages in *S. jarrovii* exhibit no clear conservation of
362 these sex-biased expression patterns across other phrynosomatid species (Fig. 7C). Overall, these
363 evolutionary patterns of sex-biased gene expression indicate that the 1.76-Mbp distal region of
364 chromosome 10 is a recently X-linked region in *S. undulatus* (and closely related species such as
365 *S. tristichus*, Fig. 1B), and that the 11-Mbp distal region of chromosome 6 in *S. undulatus* has
366 also recently become sex-linked in the lineage represented here by *S. jarrovii* (Fig. 7C).

Discussion

Recent research on sex chromosomes has emphasized the distinction between dosage compensation (of X or Z with autosomes in the heterogametic sex) and expression balance (of X or Z between the sexes) while noting that associations between the two can differ across lineages (Bista et al. 2021; Gu and Walters 2017; Saunders and Muyle 2024). In *Sceloporus undulatus,* male-female expression imbalance across the ancestral, male-hemizygous region of X appears to be associated with the overexpression of this region (relative to autosomes) in females, rather than its underexpression in males. Although this "Type IV" profile (*i.e.,* dosage compensation without male-female expression balance, following Gu & Walters 2017) has been observed in a variety of taxa (Allen et al. 2013; Muyle et al. 2018; Prince et al. 2010; Schultheiß et al. 2015), several subsequent studies have attributed it to artifacts from microarray data, the inclusion of gonadal tissue, or the lack of appropriate tests for dosage compensation (Gu and Walters 2017; Saunders and Muyle 2024). These first two concerns are not relevant to our study, but it has been proposed that tests for dosage compensation should ideally compare expression between sex-linked genes and their orthologs still in the ancestral autosomal state (Bista et al. 2021; Gu and Walters 2017). Due to the considerable age (>100 Mya) of the iguanian X chromosome that is ancestral to Pleurodonta (Acosta et al. 2019; Davalos-Dehullu et al. 2023; Marin et al. 2017), this would require comparisons across distantly related lineages in which transcriptomic profiles may have diverged considerably over millenia. Instead, by comparing X to null distributions sampled from contiguous autosomal blocks within the same genome (and the same biological replicates), we provide an alternative approach that suggests an overall Type IV expression profile for the ancestral region of the X chromosome in *S. undulatus*. We emphasize that this is a summary categorization across hundreds of X-linked genes that vary considerably in their degrees of male-

390 female expression balance, and potentially also in their corresponding degrees of dosage
391 compensation in males. Individual sex-linked genes can vary in whether they exhibit Type I-IV
392 expression profiles (Saunders and Muyle 2024; Webster et al. 2024), even in squamate reptiles
393 with mechanisms for near-complete dosage compensation, such as *Anolis carolinensis* (Marin et
394 al. 2017; Rupp et al. 2017). Interestingly, the same Type IV pattern of male-female expression
395 imbalance appears to characterize the more recently X-linked distal region of the *S. undulatus* X
396 chromosome (DR10). However, it is unclear whether Y degeneration has proceeded to the extent
397 that males actually require dosage compensation for most of this neo-X region, given that $\log_2$
398 male/female DNA coverage ranges from 0 to -1 for individual genes in DR10 and that not at all
399 genes may actually require compensation given their biological function.

400 In contrast to the ancestral region of the X chromosome, the distal region of *S. undulatus*
401 chromosome 6 (DR6) that we identify as a putative neo-X region in *S. jarrovii* appears to exhibit
402 an overall "Type III" expression profile, corresponding to the lack of dosage compensation in
403 males and the lack of expression balance between sexes. This pattern is common in ZW systems,
404 including other squamate reptiles (Rovatsos et al. 2019; Webster et al. 2024), but rare in XY
405 systems (Gu and Walters 2017; Saunders and Muyle 2024). Nonetheless, our comparisons of
406 DR6 expression against randomly sampled autosomal blocks from *S. jarrovii* and also against
407 orthologs in the ancestral autosomal state in *S. undulatus* both indicate that DR6 in *S. jarrovii* is
408 expressed at typical autosomal levels in females and at substantially lower levels in males. Such
409 Type III expression profiles may correspond to early evolutionary stages in which degeneration
410 of Y has created dosage effects in males, but mechanisms for compensatory upregulation of X
411 have yet to evolve. Likewise, Type IV expression profiles may correspond to later evolutionary
412 stages in which dosage compensation has been achieved via the upregulation of X in males, but

413 male-female expression imbalance persists due to the concomitant upregulation of X in females.
414 Ohno (1967) hypothesized that this state may precede the evolution of mechanisms such as X-
415 inactivation in females, which then restore male-female expression balance (Grant et al. 2012;
416 Marin et al. 2017). However, it is unclear whether "Type I" patterns characterized by dosage
417 compensation and male-female expression balance actually evolve via this proposed sequence,
418 particularly in vertebrates (Gu and Walters 2017; Saunders and Muyle 2024). While many
419 ancestrally X-linked genes do exhibit both dosage compensation and male-female expression
420 balance in *S. undulatus*, it is clear that many others still lack male-female expression balance
421 despite sufficient time for its evolution in this ancient (>100 Mya) XY system.

422 The anolid lizard *Anolis carolinensis* has a *Drosophila*-like epigenetic mechanism for the
423 male-specific upregulation of hemizygous X-linked genes (Marin et al. 2017), producing a Type
424 I pattern of both dosage compensation and male-female expression balance across the majority
425 of the X chromosome (Chen et al. 2020a; Rovatsos and Kratochvíl 2021; Rupp et al. 2017). This
426 is noteworthy as one of the few examples of near-complete dosage compensation accompanied
427 by near-complete male-female expression balance in any vertebrate (Chen et al. 2020a; Metzger
428 et al. 2021; Saunders and Muyle 2024). Intriguingly, recent analyses of the phrynosomatid
429 lizards *Urosaurus nigricaudus* and *U. bicarinatus* suggested both dosage compensation and
430 male-female expression balance across X, raising the possibility that the epigenetic mechanism
431 for male-specifc upregulation of X that was first discovered in *A. carolinensis* may be broadly
432 conserved across these distantly related families in Pleurodonta that share a homologous X
433 chromosome (Davalos-Dehullu et al. 2023). Our results are only partly consistent with this
434 interpretation. Although we find that the ancestral region of X does exhibit complete (brain,
435 muscle) to partial (liver) dosage compensation relative to autosomes in *S. undulatus* males, we

436 also find clear evidence of widespread male-female expression imbalance for this same ancestral
437 region of X across phrynosomatids, including another *Urosaurus* species, *U. ornatus.*
438 This discrepancy between studies is unlikely to reflect differences in the genomes used
439 for read mapping (*U. nigricaudus* versus *S. undulatus*), as both produce clear signatures of male
440 hemizygosity for the ancestral region of X when mapping genomic DNA. However, whereas we
441 set out to explicitly test for differential expression on a gene-by-gene basis by calculating mean
442 male and female expression levels from multiple replicate libraries (n = 5-7 per sex) across
443 multiple ages and tissues, Davalos-Dehullu et al. (2023) derived male-female expression ratios
444 from pairwise combinations of one individual male library against one individual female library
445 (n = 2 libraries total per sex). This difference in methodology and sample size, potentially in
446 combination with our use of isolated tissues (brain, liver, and muscle) rather than tail samples
447 comprised of multiple tissue types (*e.g.,* bone, muscle, skin), may have afforded us greater power
448 and precision for identifying sex-biased expression. Importantly, we note that the majority of
449 genes on X lack sex-biased expression for most ages and most tissues, and several even exhibit
450 consistently male-biased expression despite their hemizygosity in males. Therefore, much of the
451 X chromosome does appear to exhibit both dosage compensation and at least partial male-female
452 expression balance in phrynosomatids, despite the clear lack of male-female expression balance
453 for dozens of individual genes. Even those genes that are consistently female-biased across ages
454 and tissues have mean expression ratios of 1.7 rather than 2-fold, indicating partial expression
455 balance. In this sense, *S. undulatus* and other phrynosomatids appear similar to many other
456 species in which dosage compensation is partial and occurs on a gene-by-gene basis (Furman et
457 al. 2020; Gu and Walters 2017; Mank 2013, 2009; Mank and Ellegren 2009; Mullon et al. 2015).

458 This is true even for the near-complete dosage compensation and male-female expression
459 balance seen in *A. carolinensis* (Marin et al. 2017; Rupp et al. 2017; Saunders and Muyle 2024).
460 Chromosomal fusions are common in *Sceloporus* (Leaché et al. 2016), particularly for
461 sex chromosomes (Lisachov et al. 2021). It has been proposed that pseudoautosomal regions
462 (PARs) on the tips of sex chromosomes may facilitate such fusions by avoiding the creation of
463 multiple sex chromosome systems, since the newly fused, formerly autosomal segment can be
464 transferred to the other sex chromosome (*e.g.*, from X to Y) by recombination (Lisachov et al.
465 2021). Although we cannot assess the structure of the putative X-autosome translocation from
466 chromosome 6 to 10 in *S. jarrovii*, the fusion that formed DR10 in the *S. undulatus* lineage is
467 located adjacent to a small region of ancestrally X-linked genes with balanced DNA coverage
468 and expression between the sexes, suggesting that the fusion occurred at a terminal PAR.
469 Interestingly, many of the same syntenic blocks of genes have been repeatedly involved in
470 fusions with sex chromosomes across squamate reptiles (Lisachov et al. 2021), and the DR10
471 region in *S. undulatus* provides another example of this phenomenon. DR10 maps to a portion of
472 a putatively autosomal michrochromosome in other phrynosomatid genomes, but the entire
473 microchromosome has undergone an independent fusion with X in the anolid *A. sagrei* (Geneva
474 et al. 2022; Giovannotti et al. 2017; Kichigin et al. 2016).
475 Finally, our study illustrates how the transcriptomic signatures of male-female expression
476 imbalance can both generate and test hypotheses about the evolution of sex chromosomes, even
477 in the absence of genomic or karyotypic data. For example, the phylogenetically conserved
478 pattern of male-female expression imbalance for genes that map to the ancestrally X-linked
479 region of *S. undulatus* chromosome 10 supports the hypothesis that this region has remained
480 largely X-linked throughout phrynosomatid evolution, with the possible exception of *S. sleveni*.

481 By contrast, the distal region of chromosome 10 (DR10) only exhibits this signature of male-
482 female expression imbalance in *S. undulatus,* consistent with the hypothesis that this region
483 became X-linked more recently, after the split between lineages that gave rise to *S. undulatus*
484 and *S. virgatus*. Syntenty analyses indicate that this region is also X-linked in *S. tristichus*,
485 suggesting that it fused with the ancestral X chromosome approximately 6-10 Mya based on
486 divergence estimates for these three species (Leaché et al. 2016; Westfall et al. 2021). We also
487 found a strong signature of male-female expression imbalance in *S. jarrovii* for genes that map to
488 a small region of *S. undulatus* chromosome 6 (DR6), and the absence of this signature from all
489 other species in our analysis supports the hypothesis that DR6 is also a recently X-linked region.
490 Given that male-female expression imbalance is pronounced and male expression appears to lack
491 dosage compensation for DR6 in *S. jarrovii*, this may represent a younger neo-X region than
492 DR10. However, our current transcriptome sampling across *Sceloporus* lacks the phylogenetic
493 resolution to estimate its age more precisely. In future comparative work, tests for transcriptomic
494 signatures of male-female expression imbalance could provide an efficient way to identify and
495 date similar X-autosome fusions in this and other lineages, particularly when sequencing tissues
496 or ages that exhibit relatively little sex-biased expression from other regulatory mechanisms.
497

498 **Materials and Methods**

499 Synteny and Dosage of the *S. undulatus* X Chromosome

500 To confirm inferences from several previous studies (Davalos-Dehullu et al. 2023;
501 Westfall et al. 2021), we assessed the synteny of *S. undulatus* chromosome 10 (NC_056531.1)
502 with the genomes of three other iguanian lizards in the Pleurodonta clade that share an ancient
503 (>100 Mya) X chromosome: *Phrynosoma platyrhinos* (GCA_020142125.1, MUOH_PhPlat_1.1,

504 (Koochekian et al. 2022)), *Anolis carolinensis* (GCF_000090745.2, AnoCar2.0, (Alföldi et al.
505 2011)), and *Anolis sagrei* (GCA_025583915.1, AnoSag2.1, (Geneva et al. 2022)). Each of these
506 other three genomes was sequenced and assembled from a female specimen. The ancestral X
507 chromosome for this lineage has undergone multiple fusions with autosomes to form several
508 more recently X-linked strata in *A. sagrei* (Geneva et al. 2022). Given the phylogenetic distance
509 separating the species in our analyses (common ancestor ca. 83 Mya), we determined orthology-
510 based syntenic relationships using the R package *GENESPACE* (Lovell et al. 2022), which aligns
511 amino acid sequences using *DIAMOND2* (Buchfink et al. 2015), identifies orthogroups with
512 *OrthoFinder* (Emms and Kelly 2019, 2015), and determines syntenic regions for each non-
513 reciprocal pair of genomes by collapsing syntenic orthogroups into a pan-genome annotation.
514 *GENESPACE* identified a minimum of 16,657 genes distributed across 15,662 orthogoups in *P.*
515 *platyrhinos* and a maximum of 28,605 genes distributed across 15,458 orthogroups in *A.*
516 *carolinensis* after filtering for overdispersion. We used the *GENESPACE* function 'plot_riparian'
517 to visualize synteny for the *S. undulatus* genome with specific focus on chromosome 10.
518 To precisely resolve synteny of the X chromosome at the same gene-by-gene resolution
519 as our transcriptomic analyses, we conducted BLASTN (Altschul et al. 1990; Madden 2013)
520 searches using the longest annotated transcript for each gene on *S. undulatus* chromosome 10 (*n*
521 = 330 with XM accessions) as a query against the NCBI reference genomes of five other
522 iguanian lizards in Pleurodonta: closely related *Sceloporus tristichus,* which was formerly
523 considered a subspecies of *S. undulatus* (GCA_016801065.1, ASM1680106v1 (Bedoya and
524 Leaché 2021)), the additional phrynosomatids *Urosaurus nigricaudus* (GCA_034509955.1,
525 ASU_Unig_1 (Davalos-Dehullu et al. 2023)) and *Phrynosoma platyrhinos* (GCA_020142125.1,
526 MUOH_PhPlat_1.1 (Koochekian et al. 2022)), and two more distantly related anolids, *Anolis*

527 *sagrei* (GCA_037176765.1, rAnoSag1) and *A. carolinensis* (GCA_035594765.1, rAnoCar3.1).
528 We used default BLASTN parameters with minor modifications (reward = 1, penalty = 2, and
529 word_size = 28) and sorted results by lowest e-value and highest query coverage. Across every
530 search, the top three hits were always from the same gene, so we used the top BLASTN hit for
531 each transcript to infer the chromosomal location of the homologous gene in each of the other
532 five species.

533 To characterize sex differences in dosage, we used NCBI *sratoolkit* v.3.0.5 to download
534 short-read, whole-genome sequences (Illumina paired-end 150 bp reads) from 18 female and 11
535 male *S. undulatus* specimens obtained by Assis et al. (2025) as part of a separate study (NCBI
536 accession numbers SRR12504882 to SRR12504910 within bioproject PRJNA656311). We
537 trimmed adaptors and filtered low-quality reads used *fastp* (Chen et al. 2018) with default
538 settings, then summarized quality control metrics using *multiqc* (Ewels et al. 2016). Samples had
539 a mean duplication rate of 8.8% and we retained a mean of 319 M reads per sample (>95% of
540 input) after filtering. We aligned reads to the *S. undulatus* genome using *bowtie2* (Langmead and
541 Salzberg 2012) with default settings and removed alignments with a mapping quality (MQ) score
542 below 20 using *samtools* (Li et al. 2009). The alignment rate exceeded 95% for all specimens.
543 We estimated per-base pair depth of coverage for each individual with 'genomeCoverageBed'
544 and calculated the mean depth of coverage for each sex over non-overlapping 100-kbp windows
545 across the entire genome using 'map' from *bedtools* (Quinlan and Hall 2010). To correct for
546 differences in sequencing depth across individuals, we weighted each 100-kbp window value by
547 the genome-wide mean depth of coverage for that individual using custom *awk* functions.
548 Individuals were sequenced at 54x coverage on average, with normalized depth of coverage

549 ranging from 0.88 (chromosome 11) to 1.02 (chromosome 8) in females and 0.56 (chromosome
550 10) to 1.03 (chromosome 8) in males.

551 To calculate a per-gene weighted coverage value, we first divided the mean coverage
552 depth across the open reading frame of each gene by the mean depth of coverage of its
553 chromosome or scaffold in each individual. Next, we caculated the mean weighted coverage per
554 gene, per sex. We then calculated $\log_2$ (mean weighted coverage in males + 0.001 / mean
555 weighted coverage in females + 0.001) for each gene, which we refer to as $\log_2$ (male/female)
556 coverage. X-linked genes that are hemizygous in males should have $\log_2$ (male/female) coverage
557 values near -1. Although the *S. undulatus* genome was sequenced from a male specimen, it does
558 not contain an assembled Y chromosome (Westfall et al. 2021). To identify potential Y-liked
559 genes, we searched for any scaffolds containing at least one annotated gene with a mean $\log_2$
560 (male/female) coverage value greater than 0.5. To identify potential X-liked genes that were not
561 assembled with chromosome 10, we searched for any scaffolds containing at least one annotated
562 gene with a mean $\log_2$ (male/female) coverage value less than -0.5.

563

564 Tissue Collection for Gene Expression

565 To describe sex differences in gene expression, we collected tissues immediately upon
566 capture of wild animals in their natural habitats. All procedures were reviewed and approved by
567 the Institutional Animal Care and Use Committees at the University of Virginia (protocol 3896),
568 Florida International University (IACUC-20-012-CR01), and Rutgers University (PROTO
569 201800157). Animals were collected under permits from Arizona Game and Fish (SP658032 and
570 SP407104), Texas Parks and Wildlife (SPR-0719-113), and New Jersey Fish and Wildlife (SC
571 2019007). Additional collecting and land use permissions were obtained from Catalina State

572 Park (AZ), the Coronado National Forest branch of the United States Forest Service (AZ),
573 Tucson Parks and Recreation (AZ), Dalquest Desert Research Station (TX), and Colliers Mills
574 Wildlife Management Area (NJ). Collecting locations are provided in Table S1.

575 We collected *S. undulatus* and *S. jarrovii* at each of three ages: neonate, maturing, and
576 adult (n = 5-7 individuals per age, per sex; Table S1). Neonates were collected within several
577 weeks of hatching in oviparous, spring-breeding *S. undulatus* (early September, age <1 mo) and
578 within several weeks of birth in viviparous, fall-breeding *S. jarrovii* (mid June, age <1 mo).
579 Maturing individuals were sampled when sex differences in growth, coloration, and circulating
580 testosterone first emerge in the summer after hatching in *S. undulatus* (July, age 10-11 mo) and
581 the first fall breeding season after birth in *S. jarrovii* (late September, age 4-5 mo) (Cox and
582 John-Alder 2007, 2005; Cox et al. 2005). Reproductive adults were sampled during the breeding
583 season in both *S. undulatus* (mid May, age >20 mo) and *S. jarrovii* (late September, age >16
584 mo). To assess the evolution of sex-biased gene expression, we also collected reproductive adults
585 of five additional *Sceloporus* species (*S. clarkii, S. magister, S. merriami, S. slevini, S. virgatus*)
586 and three species representing other phrynosomatid genera (*Cophosaurus texanus, Urosaurus*
587 *ornatus*, *Uta stansburiana*; n = 6 per sex, per species). Adults of each species were sampled in
588 late April or early May during their breeding seasons (Table S1).

589 We captured lizards by hand or using a hand-held pole with a loop of braided fishing line,
590 then immediately measured them for mass (nearest 0.1 g) and snout-vent length (nearest 1 mm).
591 Sex was determined according to presence or absence of enlarged post-anal scales (present only
592 in males) and confirmed by inspection of the gonads during tissue collection. Immediately
593 following measurement, we euthanized lizards via decapitation and collected liver, whole brain,

594 and muscle (along the femur) into RNAlater (Qiagen, Valencia, CA, USA) on ice. Tissues were
595 held overnight at 4°C, frozen at -20°C, and then stored at -80°C until RNA extraction.
596
597 RNA Extraction and Sequencing
598 We extracted total RNA from liver for all 10 species (Table S1). For *S. undulatus* and *S.*
599 *jarrovii*, this included three age groups (neonate, maturing, and adult). For *S. undulatus*, we also
600 extracted RNA from brain and muscle from all three age groups. RNA was extracted using the
601 Illustra/Cytiva RNAspin Mini RNA Isolation Kit (Global Life Sciences Solutions USA,
602 Marlborough, MA, USA), following the manufacturer's protocol, with the exception that all
603 tissues were homogenized twice (45 s per round at 30 Hz) in lysis buffer using 5-mm stainless
604 steel beads in a Tissuelyser II bead mill (Qiagen; Germantown, MD, USA). We assessed RNA
605 concentrations for all samples using a Nanodrop spectrophotometer (ThermoFisher Scientific,
606 Waltham MA, USA). We also assessed RNA quality and concentration for most samples on an
607 Agilent Bioanalyzer (RNA 6000 Pico; Agilent Biotechnologies, Santa Clara, CA, USA). All
608 samples exhibited sufficient quality for library preparation and sequencing (mean RIN = 8.1).
609 Preparation of cDNA libraries and RNA sequencing was carried out by the Georgia
610 Genomics and Bioinformatics Core at the University of Georgia (Athens, GA, USA). Libraries
611 were prepared using the KAPA Stranded mRNA-Seq kit for Illumina platforms with poly(A)
612 selection (KAPA Biosystems; Wilmington, MA, USA). Library preparation and sequencing were
613 conducted in three batches with respect to species and tissue (Table S1) to optimize comparisons
614 between sexes and to obtain approximately 20 M reads per sample. In the first batch, libraries for
615 *S. undulatus* and *S. jarrovii* liver from all three ages were prepared together using ~1 μg total
616 RNA per sample. In the second batch, libraries for *S. undulatus* brain and muscle from all three

617 ages were prepared using ~2 μg total RNA (brain) or ~0.5 μg total RNA (muscle), with libraries
618 from each tissue loaded in equimolar ratios for sequencing. In the third batch, libraries for *S.*
619 *virgatus, S. clarkii, S. slevini, S. magister, S. merriami*, *U. ornatus*, *U. stansburiana*, and *C.*
620 *texanus* liver from adults were prepared using ~1 μg total RNA. Each batch was sequenced twice
621 on Illumina P3 flow cells (paired-end, 100-bp reads) using an Illumina NextSeq 2000.
622
623 Read Count Generation and Differential Expression Analysis
624 All RNAseq reads were assessed for quality and trimmed using *fastp* (Chen et al. 2018)
625 with paired-end base correction, low-complexity filtering, and 3' end tail quality trimming
626 (average phred score threshold = 20 and window size = 5). Poly(g) and poly(x) trimming were
627 also enabled to remove low complexity sequences from the 3' end of reads, along with an overall
628 minimum length filter of 36 bp and minimum phred quality threshold of 25. Cleaned read pairs
629 and reads orphaned during trimming (*i.e.*, read partner removed due to length or quality) were
630 aligned to the *S. undulatus* genome (GCA_019175285.1; SceUnd_v1.1) using *subread-align*
631 (Liao et al. 2013b) with *S. undulatus* RefSeq coding sequences (GCF_019175285.1) as a guide
632 during alignment (accessed via NCBI). Although we used the *S. undulatus* genome as a common
633 reference to generate comparable read counts across all 10 species, we note that the genus
634 *Sceloporus* exhibits widespread chromosomal evolution (Leaché et al. 2016), such that gene
635 locations in other species may differ from those in the *S. undulatus* assembly.
636 For all reads from *Sceloporus* species, we used default parameters in *subread-align* to
637 identify valid alignments to coding regions in the *S. undulatus* genome. For *Urosaurus*, *Uta*, and
638 *Cophosaurus*, we relaxed alignment stringencies due to increased phylogenetic distance and
639 reduced alignment rates observed when default parameters were used. This entailed a lower

640 minimum number of subreads necessary to report an alignment (-m 2), an increased number of
641 mismatches allowed (-M 5), a lower minimum fragment size (-d 35), an increased maximum
642 fragment size (-D 750), and an increased maximum number of indels (-I 7). Paired reads and
643 reads orphaned during *fastp* trimming were aligned independently and expression counts for all
644 species were generated from alignments using *featureCounts* (Liao et al. 2013a) with default
645 parameters. We summed expression counts from paired reads and orphaned reads to generate
646 final expression estimates for each sample. Only unique alignments were counted towards the
647 total expression estimate for a gene (*i.e.,* multi-mapping reads were not counted).

648 We conducted differential expression analyses using R (v 4.1.1) (R Core Team, 2019)
649 package *edgeR* (Chen et al. 2016; McCarthy et al. 2012; Robinson et al. 2009; Robinson and
650 Smyth 2007). Prior to analysis, we filtered counts to remove low-expression genes using *edgeR*
651 function 'FiltrByExpr' separately for each tissue within each species (Table S1, "edgeR model").
652 To identify and remove outlier libraries after low-expression filtering, we applied a TMM
653 (trimmed mean of M-values) normalization to expression counts in *edgeR*, then used a $\log_{10}$
654 counts-per-million (CPM) transformation to adjust for library size. We used robust PCA on $\log_{10}$
655 (CPM) values to identify and remove any outlier libraries using R package *rrcov* and function
656 'PcaGrid' (crit.pca.distance = 0.975) (Chen et al. 2020b). We conducted outlier analyses
657 separately for each tissue within each species. The total numbers of samples passing outlier
658 filtering are reported in Table S1. Following outlier removal, we conducted differential
659 expression analysis using TMM-normalized read counts, which we fit to a negative binomial
660 model (*edgeR* function 'glmQLFit', robust = TRUE) with separate models for each species. We
661 identified sex-biased DEGs (differentially expressed genes) using quasi-likelihood *F*-tests
662 comparing female versus male expression for each species with *edgeR* function 'glmQLFTest'.

663 Within each species, we made pairwise comparisons between sexes for each combination of age
664 and tissue. Genes with a Benjamini-Hochberg *P*-value adjusted for the transcriptome-wide false
665 discovery rate ("FDR") < 0.05 were considered DEGs (Benjamini and Hochberg 1995).
666
667 Testing for Male-Female Expression Imbalance in *S. undulatus*
668 After identifying significantly sex-biased DEGs within each combination of age and tisse,
669 we identified the subsets of genes that are consistently female-biased or consistently male-biased
670 DEGs across all ages within a tissue, then determined the chromosomal locations of these genes
671 in the *S. undulatus* assembly. If consistently female-biased DEGs are the result of male-female
672 dosage imbalance, then these DEGs should map predominantly to chromosome 10, the X
673 chromosome. If consistently male-biased DEGs are the result of Y-linkage, then these DEGs
674 should map predominantly to unplaced scaffolds in the *S. undulatus* assembly, which does not
675 include an assembled Y chromosome but does contain sequence from a male specimen. Mapping
676 of consistently sex-biased DEGs to autosomes (chromosomes 1-9 and 11) would indicate either
677 an error in sex chromosome assembly, or a mechanism for consistently sex-biased expression
678 other than dosage imbalance due to male hemizygosity. As noted above, we assessed $\log_2$
679 male/female DNA coverage for each of these consistently sex-biased DEGs to infer underlying
680 patterns of dosage. We also visually assessed genome-wide patterns of sex-biased expression
681 using Mahattan plots with the $-\log_{10}$ (*P*-value) of differential expression for each gene ordered
682 sequentially by chromosome number and transcriptional start site.
683 As a complementary approach to our DEG analysis, we assessed chromosome-wide
684 patterns of sex-biased expression by using *edgeR* function 'rpkm' to calculate the expression of
685 each gene as FPKM (fragments per kilobase of transcript per million mapped reads) using *S.*

686 *undulatus* gene lengths (GCF_019175285.1). For each tissue, we used Wilcoxon signed-rank
687 tests with a Bonferroni-adjusted alpha (0.05 / 3 = 0.017) to test whether the median sex bias in
688 expression ($\log_2$ male/female FPKM) of genes on chromosome 10 differed significantly from 0.
689 We conducted these analyses both with and without the subsets of consistently sex-biased DEGs
690 previously identified in each tissue (see above). Because the current *S. undulatus* assembly does
691 not include a unique Y scaffold, we could not conduct similar tests for Y-linked expression.
692
693 Confirming Male-Female Expression Imbalance in *S. undulatus* Using the *S. tristichus* Genome
694 Because the assembly of the *S. undulatus* X chromosome may have been influenced by
695 homologous reads from Y (Westfall et al. 2021), we repeated our analyses of differential gene
696 expression by aligning RNAseq reads from *S. undulatus* to the genome of a closely related
697 congener (*Sceloporus tristichus,* formerly *S. undulatus tristichus*) that was sequenced exclusively
698 from female tissue (Bedoya and Leaché 2021). Using this assembly should minimize any
699 artifacts potentially introduced by similar X and Y sequences in the *S. undulatus* genome, such
700 as the co-assembly of X and Y gametologs on chromosome 10 or the failure of X gametologs to
701 assemble on chromosome 10. Read alignments and estimates of gene expression were made
702 using subread-align and featureCounts against the *S. tristichus* genome (ASM1680141v1) and
703 gene annotations from Bedoya and Leaché (2021; Sceloporus_tristichus_snow_11.gff3) with the
704 same parameters used during alignment to the *S. undulatus* genome (described above).
705
706 Identification of Potential Gametolog Pairs in *S. undulatus*
707 If males express two formerly allelic copies of the same gene (*i.e.*, X and Y gametologs),
708 then the independent mapping of reads to each gametolog could create the appearance of female-

709 biased expression of the X gametolog for a gene that is otherwise expressed similarly in both
710 sexes. For all genes identified as consistently sex-biased DEGs using the *S. undulatus* genome,
711 we used BLASTN (Madden 2013) to search for similar sequences that could represent potential
712 gametologs. We used the longest annotated transcripts for each consistently female-biased DEG
713 as query sequences and searched them against the *S. undulatus* (taxid:8520) refseq_rna database
714 using default alignment parameters (E-threshold = 0.05; word size = 11; max matches in query =
715 0; match/mismatch scores = 2,-3; gap costs = Existence: 5, Extension: 2) with low-complexity
716 filters enabled. We queried the top 100 hits for each female-biased DEG sequence to identify any
717 located on unassembled scaffolds, then assessed male and female expression levels (FPKM) to
718 identify those with low expression in females, indicating possible Y gametologs. We applied a
719 similar strategy to identify any potential X gametologs for consistently male-biased DEGs,
720 which would be expected to occur on chromosome 10 or unplaced scaffolds. In situations where
721 we identified a potential gametolog pair, we re-assessed patterns of sex bias after pooling reads
722 from each separately assembled region (*i.e.*, summing putative X and Y gametolog reads).
723
724 Comparing X-linked to Autosomal Expression in *S. undulatus*
725 We established null distributions of median autosomal expression by randomly sampling
726 spatially contiguous blocks of the same number of autosomal genes as expressed genes on X. We
727 calculated the median $\log_2$ FPKM expression for each block of genes in each tissue, age, and sex,
728 repeating this random selection process 1000 times throughout the autosomal genome to generate
729 a null distribution of median autosomal expression for each combination of tissue, age, and sex.
730 For each sampling iteration, we selected a contiguous block of genes on the same scaffold
731 (excluding genes on unplaced scaffolds) and arrayed consecutively by start position, similar to

732 the arrangement of genes on X. Each block of autosomal genes was sampled only once to avoid
733 pseudoreplication. We then tested whether the median $\log_2$ FPKM expression of genes on X fell
734 outside the lower 5% or upper 95% quantiles of the corresponding autosomal distribution. If
735 median expression on X falls below the corresponding null distribution of median autosomal
736 expression in males, this would indicate a lack of dosage compensation ("Type III" expression
737 pattern, Gu and Walters 2017). If the median expression of genes on X falls above the
738 corresponding null distribution in females, this could indicate that dosage compensation in males
739 has resulted in overexpression of X in females ("Type IV" expression pattern; Gu and Walters
740 2017). We conducted these tests separately for genes on the ancestrally X-linked, 14.85-Mbp
741 region of chromsosome 10 (n = 231 to 255 expressed genes, depending upon tissue), as well as
742 the more recently X-linked, 1.76-Mbp distal region of chromosome 10 (n = 41 to 46 expressed
743 genes), with null distributions of autosomal expression generated separately for each region
744 based on its number of expressed genes in each tissue.
745
746 Testing for Male-Female Expression Imbalance in *S. jarrovii*
747 For *S. jarrovii*, we used the same methods described above for *S. undulatus* to identify
748 consistently sex-biased genes in the liver (i.e., significant DEGs biased towards the same sex
749 across all three ages), and to test for overall male-female expression imbalance across genes on
750 chromosome 10 in the *S. undulatus* assembly (*i.e.*, significant deviations of median $\log_2$
751 male/female FPKM ratios from 0 using Wilcoxon signed-rank tests with Bonferroni correction
752 for tests across 3 ages). Because the distal 1.76-Mbp portion of *S. undulatus* chromosome 10
753 (DR10) is presumably autosomal in *S. jarrovii*, we tested for male-female expression imbalance

754 separately in DR10 and in the ancestrally X-linked 14.85-Mbp region of chromosome 10, which
755 we expected to be X-linked in both species.
756 Our analyses in *S. jarrovii* unexpectedly uncovered a signal of highly sex-biased
757 expression in genes mapping to a small (~11 Mbp) distal region on chromosome 6 in the *S.*
758 *undulatus* assembly (hereafter "DR6"), so we conducted additional analyses to test whether this
759 region exhibits the transcriptomic signatures of an X chromosome in *S. jarrovii*. We used
760 Wilcoxon signed-rank tests (as described above for chromosome 10) to test whether the median
761 $\log_2$ male/female FPKM expression ratio for genes on DR6 differs from 0, and also to compare
762 (separately within each sex) the median $\log_2$ FPKM expression of genes in DR6 to null
763 distributions of median $\log_2$ FPKM expression for 1000 randomly sampled genes located
764 contiguously in other autosomal regions. For comparison, we conducted similar analyses of DR6
765 in *S. undulatus,* where it is autosomal. To directly test for an evolutionary reduction in
766 expression of DR6 genes in *S. jarrovii* males, as expected if this formerly autosomal region has
767 become X-linked but still lacks complete dosage compensation, we conducted paired (by gene) *t*-
768 tests comparing expression of DR6 homologs between *S. undulatus* and *S. jarrovii*. We predicted
769 that expression of DR6 would be similar in females of each species, but reduced in *S. jarrovii*
770 males relatieve to *S. undulatus* males.
771
772 <u>Characterizing the Evolution of Gene Expression Across Phrynosomatidae</u>
773 We generated liver transcriptomes for adult males and females of 7 *Sceloporus* species,
774 plus representatives of 3 other phrynosomatid genera (n = 5-7 individuals per sex, per species;
775 Table S1). For species, we tested whether genes that map to the ancestrally X-linked, male-
776 hemizygous, 14.85-Mbp region of chromosome 10 in the *S. undulatus* assembly exhibit female-

biased expression. To resolve the evolution of neo-X regions, we also tested whether genes that map to the distal regions of *S. undulatus* chromosome 10 (DR10, putative neo-X region in *S. undulatus*) and chromosome 6 (DR6, putative neo-X region in *S. jarrovii*) exhibit female-biased expression in any other species. For each comparison described above, we used a 1-sample Wilcoxon signed-rank test with Bonferroni correction for the 10 comparisons across species (adjusted alpha = 0.005) to test for male-female dosage imbalance (median $\log_2$ male/female FPKM < 0) of all expressed genes that map to the corresponding regions of the *S. undulatus* assembly. We also conducted similar analyses using only the subsets of consistently female-biased DEGs from chromosome 10 (*i.e.,* DEGs in *S. undulatus* transcriptomes) or DR6 (*i.e.,* DEGs in *S. jarrovii* transcriptomes). We visualized evolutionary patterns in gene expression using a consensus phylogeny based on several sources (Leaché et al. 2016; Pyron et al. 2013).

Acknowledgments

We thank Matt Watson and Tyler Wittman for help with sample collection. We thank the Georgia Genomics and Bioinformatics Core (GGBC) for library preparation and sequencing. The authors acknowledge Research Computing at The University of Virginia (https://rc.virginia.edu) for providing compulational resources and technical support that have contributed to the results reported within this publication. This work was supported by a Collaborative Research award from the U.S. National Science Foundation (IOS 1755134 to CLC, IOS 1754934 to HBJ-A, and IOS 1755026 to RMC). CDR was supported by a Research Traineeship from the U.S. National Sceince Foundation (NRT-ROL 2021791). PLHM was supported by a Rising Scholars Postdoctoral Fellowship from the University of Virginia.

Data Availability

RNAseq data underlying this article will be made available through the National Center for Biotechnology Information (NCBI) Short Read Archive upon acceptance. Read counts and other data will be publicly available.

Literature Cited

Acosta A, et al. 2019. Corytophanids replaced the pleurodont XY system with a new pair of XY chromosomes. Genome Biol Evol. 11(9): 2666-2677. doi: 10.1093/gbe/evz196

Alam SMI, Sarre SD, Gleeson D, Georges A, Ezaz T. 2018. Did lizards follow unique pathways in sex chromosome evolution? Genes. 9(5). doi: 10.3390/genes9050239

Albritton SE, et al. 2014. Sex-biased gene expression and evolution of the X chromosome in nematodes. Genetics. 197(3): 865-883. doi: 10.1534/genetics.114.163311

Alföldi J, et al. 2011. The genome of the green anole lizard and a comparative analysis with birds and mammals. Nature. 477(7366): 587-591. doi: 10.1038/nature10390

Allen SL, Bonduriansky R, Chenoweth SF. 2013. The genomic distribution of sex-biased genes in *Drosophila serrata*: X chromosome demasculinization, feminization, and hyperexpression in both sexes. Genome Biol Evol. 5(10): 1986-1994. doi: 10.1093/gbe/evt145

Altmanova M, et al. 2018. All iguana families with the exception of basilisks share sex chromosomes. Zoology. 126(98-102. doi: 10.1016/j.zool.2017.11.007

Altschul SF, Gish W, Miller W, Myers EW, Lipman DJ. 1990. Basic local alignment search tool. 215(3): 403-410. doi: 10.1016/S0022-2836(05)80360-2

822 Assis BA, et al. 2025. Genomic signatures of adaptation in native lizards exposed to human-
823 introduced fire ants. 16(1): 89. doi: 10.1038/s41467-024-55020-4
824 Bachtrog D, et al. 2011. Are all sex chromosomes created equal? Trends Genet. 27(9): 350-357.
825 doi: 10.1016/j.tig.2011.05.005
826 Bedoya AM, Leaché AD. 2021. Characterization of a pericentric inversion in plateau fence
827 lizards (*Sceloporus tristichus*): evidence from chromosome-scale genomes. G3: Genes,
828 Genomes, Genetics. 11(2). doi: 10.1093/g3journal/jkab036
829 Benjamini Y, Hochberg Y. 1995. Controlling the false discovery rate: A practical and powerful
830 approach to multiple testing. 57(1): 289-300. doi: 10.1111/j.2517-6161.1995.tb02031.x
831 Birchler JA, Riddle NC, Auger DL, Veitia RA. 2005. Dosage balance in gene regulation:
832 Biological implications. Trends Genet. 21(4): 219-226. doi: 10.1016/j.tig.2005.02.010
833 Bista B, Wu Z, Literman R, Valenzuela N. 2021. Thermosensitive sex chromosome dosage
834 compensation in ZZ/ZW softshell turtles, *Apalone spinifera*. Philos Trans R Soc Lond B
835 Biol Sci. 376(1833): 20200101. doi: 10.1098/rstb.2020.0101
836 Buchfink B, Xie C, Huson DH. 2015. Fast and sensitive protein alignment using DIAMOND.
837 Nat Methods. 12(1): 59-60. doi: 10.1038/nmeth.3176
838 Chandler CH. 2017. When and why does sex chromosome dosage compensation evolve? Ann N
839 Y Acad Sci. 1389(1): 37-51. doi: 10.1111/nyas.13307
840 Charlesworth D. 2021. The timing of genetic degeneration of sex chromosomes. Philos Trans R
841 Soc Lond B Biol Sci. 376(1832): 20200093. doi: 10.1098/rstb.2020.0093
842 Chen J, Wang M, He X, Yang JR, Chen X. 2020a. The evolution of sex chromosome dosage
843 compensation in animals. J Genet Genomics. 47(11): 681-693. doi:
844 10.1016/j.jgg.2020.10.005

845 Chen S, et al. 2014. Whole-genome sequence of a flatfish provides insights into ZW sex
846 chromosome evolution and adaptation to a benthic lifestyle. Nat Genet. 46(3): 253-260.
847 doi: 10.1038/ng.2890
848 Chen S, Zhou Y, Chen Y, Gu J. 2018. fastp: an ultra-fast all-in-one FASTQ preprocessor.
849 Bioinformatics. 34(17): i884-i890. doi: 10.1093/bioinformatics/bty560
850 Chen X, Zhang B, Wang T, Bonni A, Zhao G. 2020b. Robust principal component analysis for
851 accurate outlier sample detection in RNA-Seq data. BMC Bioinf. 21(1): 269. doi:
852 10.1186/s12859-020-03608-0
853 Chen Y, Lun AT, Smyth GK. 2016. From reads to genes to pathways: differential expression
854 analysis of RNA-Seq experiments using Rsubread and the edgeR quasi-likelihood
855 pipeline. F1000Res. 5(
856 Cox RM, John-Alder HB. 2007. Growing apart together: The development of contrasting sexual
857 size dimorphisms in sympatric *Sceloporus* lizards. Herpetologica. 63(3): 245-257. doi:
858 10.1655/0018-0831(2007)63[245:Gattdo]2.0.Co;2
859 Cox RM, John-Alder HB. 2005. Testosterone has opposite effects on male growth in lizards
860 (*Sceloporus* spp.) with opposite patterns of sexual size dimorphism. J Exp Biol. 208(24):
861 4679-4687. doi: 10.1242/jeb.01948
862 Cox Robert M, Skelly Stephanie L, John-Alder Henry B. 2005. Testosterone inhibits growth in
863 juvenile male Eastern Fence Lizards (*Sceloporus undulatus*): Implications for energy
864 allocation and sexual size dimorphism. Physiol Biochem Zool. 78(4): 531-545. doi:
865 10.1086/430226

866 Darolti I, et al. 2019. Extreme heterogeneity in sex chromosome differentiation and dosage
867 compensation in livebearers. Proc Natl Acad Sci U S A. 116(38): 19031-19036. doi:
868 10.1073/pnas.1905298116
869 Davalos-Dehullu E, et al. 2023. Chromosome-level genome assembly of the Blacktail Brush
870 Lizard, *Urosaurus nigricaudus*, reveals dosage compensation in an endemic lizard.
871 Genome Biol Evol. 15(12). doi: 10.1093/gbe/evad210
872 Deakin JE, Ezaz T. 2019. Understanding the evolution of reptile chromosomes through
873 applications of combined cytogenetics and genomics approaches. Cytogenet Genome
874 Res. 157(1-2): 7-20. doi: 10.1159/000495974
875 Dean R, Mank JE. 2014. The role of sex chromosomes in sexual dimorphism: Discordance
876 between molecular and phenotypic data. J Evol Biol. 27(7): 1443-1453. doi:
877 10.1111/jeb.12345
878 Disteche CM. 2012. Dosage compensation of the sex chromosomes. Annu Rev Genet. 46(537-
879 560. doi: 10.1146/annurev-genet-110711-155454
880 Emms DM, Kelly S. 2019. OrthoFinder: phylogenetic orthology inference for comparative
881 genomics. Genome Biol. 20(1): 238. doi: 10.1186/s13059-019-1832-y
882 Emms DM, Kelly S. 2015. OrthoFinder: solving fundamental biases in whole genome
883 comparisons dramatically improves orthogroup inference accuracy. Genome Biol. 16(1):
884 157. doi: 10.1186/s13059-015-0721-2
885 Ewels P, Magnusson M, Lundin S, Käller M. 2016. MultiQC: summarize analysis results for
886 multiple tools and samples in a single report. Bioinformatics. 32(19): 3047-3048. doi:
887 10.1093/bioinformatics/btw354

888 Furman BLS, et al. 2020. Sex chromosome evolution: So many exceptions to the rules. Genome
889 Biol Evol. 12(6): 750-763. doi: 10.1093/gbe/evaa081
890 Gamble T, et al. 2015. Restriction site-associated DNA sequencing (RAD-seq) reveals an
891 extraordinary number of transitions among gecko sex-determining systems. Mol Biol
892 Evol. 32(5): 1296-1309. doi: 10.1093/molbev/msv023
893 Geneva AJ, et al. 2022. Chromosome-scale genome assembly of the brown anole (*Anolis sagrei*),
894 an emerging model species. Commun Biol. 5(1): 1126. doi: 10.1038/s42003-022-04074-5
895 Giovannotti M, et al. 2017. New insights into sex chromosome evolution in anole lizards
896 (Reptilia, Dactyloidae). Chromosoma. 126(2): 245-260. doi: 10.1007/s00412-016-0585-6
897 Grant J, et al. 2012. Rsx is a metatherian RNA with Xist-like properties in X-chromosome
898 inactivation. Nature. 487(7406): 254-258. doi: 10.1038/nature11171
899 Graves JA. 2016. Evolution of vertebrate sex chromosomes and dosage compensation. Nat Rev
900 Genet. 17(1): 33-46. doi: 10.1038/nrg.2015.2
901 Gu L, Walters JR. 2017. Evolution of sex chromosome dosage compensation in animals: A
902 beautiful theory, undermined by facts and bedeviled by details. Genome Biol Evol. 9(9):
903 2461-2476. doi: 10.1093/gbe/evx154
904 Gu L, Walters JR, Knipple DC. 2017. Conserved patterns of sex chromosome dosage
905 compensation in the Lepidoptera (WZ/ZZ): Insights from a moth neo-Z chromosome.
906 Genome Biol Evol. 9(3): 802-816. doi: 10.1093/gbe/evx039
907 Itoh Y, et al. 2010. Sex bias and dosage compensation in the zebra finch versus chicken
908 genomes: General and specialized patterns among birds. Genome Res. 20(4): 512-518.
909 doi: 10.1101/gr.102343.109

910 Kichigin IG, et al. 2016. Evolutionary dynamics of *Anolis* sex chromosomes revealed by
911 sequencing of flow sorting-derived microchromosome-specific DNA. Mol Genet
912 Genomics. 291(1955-1966.
913 Koochekian N, et al. 2022. A chromosome-level genome assembly and annotation of the desert
914 horned lizard, *Phrynosoma platyrhinos*, provides insight into chromosomal
915 rearrangements among reptiles. Gigascience. 11(doi: 10.1093/gigascience/giab098
916 Kratochvil L, Gamble T, Rovatsos M. 2021. Sex chromosome evolution among amniotes: Is the
917 origin of sex chromosomes non-random? Philos Trans R Soc Lond B Biol Sci.
918 376(1833): 20200108. doi: 10.1098/rstb.2020.0108
919 Langmead B, Salzberg SL. 2012. Fast gapped-read alignment with Bowtie 2. Nat Methods. 9(4):
920 357-359. doi: 10.1038/nmeth.1923
921 Leaché AD, Banbury BL, Linkem CW, de Oca AN. 2016. Phylogenomics of a rapid radiation: is
922 chromosomal evolution linked to increased diversification in north american spiny lizards
923 (Genus *Sceloporus*)? BMC Evol Biol. 16(63. doi: 10.1186/s12862-016-0628-x
924 Li H, et al. 2009. 1000 genome project data processing subgroup. The sequence alignment/map
925 format and SAMtools. Bioinformatics. 25(16): 2078-2079.
926 Liao Y, Smyth GK, Shi W. 2013a. featureCounts: an efficient general purpose program for
927 assigning sequence reads to genomic features. Bioinformatics. 30(7): 923-930. doi:
928 10.1093/bioinformatics/btt656
929 Liao Y, Smyth GK, Shi W. 2013b. The Subread aligner: fast, accurate and scalable read mapping
930 by seed-and-vote. Nucleic Acids Res. 41(10): e108-e108. doi: 10.1093/nar/gkt214

931 Lisachov AP, et al. 2021. Whole-chromosome fusions in the karyotype evolution of *Sceloporus*
932 (Iguania, Reptilia) are more frequent in sex chromosomes than autosomes. Philos Trans R
933 Soc Lond B Biol Sci. 376(1833): 20200099. doi: 10.1098/rstb.2020.0099
934 Lovell JT, et al. 2022. GENESPACE tracks regions of interest and gene copy number variation
935 across multiple genomes. eLife. 11(e78526. doi: 10.7554/eLife.78526
936 Lucchesi JC, Kuroda MI. 2015. Dosage compensation in *Drosophila*. Cold Spring Harb Perspect
937 Biol. 7(5). doi: 10.1101/cshperspect.a019398
938 Madden T. 2013. The BLAST sequence analysis tool. The NCBI handbook. 2(5): 425-436.
939 Mank JE. 2022. Are plant and animal sex chromosomes really all that different? Philos Trans R
940 Soc Lond B Biol Sci. 377(1850): 20210218. doi: 10.1098/rstb.2021.0218
941 Mank JE. 2013. Sex chromosome dosage compensation: Definitely not for everyone. Trends
942 Genet. 29(12): 677-683. doi: 10.1016/j.tig.2013.07.005
943 Mank JE. 2009. The W, X, Y and Z of sex-chromosome dosage compensation. Trends Genet.
944 25(5): 226-233. doi: 10.1016/j.tig.2009.03.005
945 Mank JE, Ellegren H. 2009. All dosage compensation is local: Gene-by-gene regulation of sex-
946 biased expression on the chicken Z chromosome. Heredity. 102(3): 312-320. doi:
947 10.1038/hdy.2008.116
948 Mank JE, Hosken DJ, Wedell N. 2011. Some inconvenient truths about sex chromosome dosage
949 compensation and the potential role of sexual conflict. Evolution. 65(8): 2133-2144. doi:
950 10.1111/j.1558-5646.2011.01316.x
951 Marin R, et al. 2017. Convergent origination of a *Drosophila*-like dosage compensation
952 mechanism in a reptile lineage. Genome Res. 27(12): 1974-1987. doi:
953 10.1101/gr.223727.117

954 McCarthy DJ, Chen Y, Smyth GK. 2012. Differential expression analysis of multifactor RNA-
955 Seq experiments with respect to biological variation. Nucleic Acids Res. 40(10): 4288-
956 4297. doi: 10.1093/nar/gks042
957 Metzger DCH, Sandkam BA, Darolti I, Mank JE. 2021. Rapid evolution of complete dosage
958 compensation in *Poecilia*. Genome Biol Evol. 13(7). doi: 10.1093/gbe/evab155
959 Mullon C, Wright AE, Reuter M, Pomiankowski A, Mank JE. 2015. Evolution of dosage
960 compensation under sexual selection differs between X and Z chromosomes. Nat
961 Commun. 6(7720. doi: 10.1038/ncomms8720
962 Muyle A, et al. 2018. Genomic imprinting mediates dosage compensation in a young plant XY
963 system. Nature plants. 4(9): 677-680.
964 Nielsen SV, et al. 2019. Escaping the evolutionary trap? Sex chromosome turnover in basilisks
965 and related lizards (Corytophanidae: Squamata). Biol Lett. 15(10): 20190498. doi:
966 10.1098/rsbl.2019.0498
967 Ohno S. 1967. Sex Chromosomes and Sex-linked Genes. Heidelberg: Springer Berlin.
968 Pennell MW, et al. 2015. Y fuse? Sex chromosome fusions in fishes and reptiles. PLOS Genet.
969 11(5). doi: 10.1371/journal.pgen.1005237
970 Pessia E, Engelstädter J, Marais GAB. 2014. The evolution of X chromosome inactivation in
971 mammals: The demise of Ohno's hypothesis? Cell Molec Life Sci. 71(8): 1383-1394.
972 doi: 10.1007/s00018-013-1499-6
973 Pinto BJ, Gamble T, Smith CH, Wilson MA. 2023. A lizard is never late: Squamate genomics as
974 a recent catalyst for understanding sex chromosome and microchromosome evolution.
975 114(5): 445-458. doi: 10.1093/jhered/esad023

976 Prince EG, Kirkland D, Demuth JP. 2010. Hyperexpression of the X chromosome in both sexes
977 results in extensive female bias of X-linked genes in the flour beetle. Genome Biol Evol.
978 2(336-346. doi: 10.1093/gbe/evq024
979 Pyron RA, Burbrink FT, Wiens JJ. 2013. A phylogeny and revised classification of Squamata,
980 including 4161 species of lizards and snakes. BMC Evol Biol. 13(1): 93. doi:
981 10.1186/1471-2148-13-93
982 Quinlan AR, Hall IM. 2010. BEDTools: A flexible suite of utilities for comparing genomic
983 features. Bioinformatics. 26(6): 841-842. doi: 10.1093/bioinformatics/btq033
984 Robinson MD, McCarthy DJ, Smyth GK. 2009. edgeR: A Bioconductor package for differential
985 expression analysis of digital gene expression data. Bioinformatics. 26(1): 139-140. doi:
986 10.1093/bioinformatics/btp616
987 Robinson MD, Smyth GK. 2007. Moderated statistical tests for assessing differences in tag
988 abundance. Bioinformatics. 23(21): 2881-2887. doi: 10.1093/bioinformatics/btm453
989 Rovatsos M, Altmanova M, Pokorna M, Kratochvil L. 2014a. Conserved sex chromosomes
990 across adaptively radiated *Anolis* lizards. Evolution. 68(7): 2079-2085. doi:
991 10.1111/evo.12357
992 Rovatsos M, et al. 2021. Do male and female heterogamety really differ in expression
993 regulation? Lack of global dosage balance in pygopodid geckos. Philos Trans R Soc
994 Lond B Biol Sci. 376(1833): 20200102. doi: 10.1098/rstb.2020.0102
995 Rovatsos M, Kratochvíl L. 2021. Evolution of dosage compensation does not depend on genomic
996 background. Molec Ecol. 30(8): 1836-1845. doi: 10.1111/mec.15853

997 Rovatsos M, Pokorna M, Altmanova M, Kratochvil L. 2014b. Cretaceous park of sex
998 determination: Sex chromosomes are conserved across iguanas. Biol Lett. 10(3):
999 20131093. doi: 10.1098/rsbl.2013.1093
1000 Rovatsos M, Rehak I, Velensky P, Kratochvil L. 2019. Shared ancient sex chromosomes in
1001 varanids, beaded lizards, and alligator lizards. Mol Biol Evol. 36(6): 1113-1120. doi:
1002 10.1093/molbev/msz024
1003 Rupp SM, et al. 2017. Evolution of dosage compensation in *Anolis carolinensis*, a reptile with
1004 XX/XY chromosomal sex determination. Genome Biol Evol. 9(1): 231-240. doi:
1005 10.1093/gbe/evw263
1006 Saunders PA, Muyle A. 2024. Sex chromosome evolution: Hallmarks and question marks. Mol
1007 Biol Evol. 41(11). doi: 10.1093/molbev/msae218
1008 Schield DR, et al. 2019. The origins and evolution of chromosomes, dosage compensation, and
1009 mechanisms underlying venom regulation in snakes. Genome Res. 29(4): 590-601. doi:
1010 10.1101/gr.240952.118
1011 Schultheiß R, Viitaniemi HM, Leder EH. 2015. Spatial dynamics of evolving dosage
1012 compensation in a young sex chromosome system. Genome Biol Evol. 7(2): 581-590.
1013 doi: 10.1093/gbe/evv013
1014 Shaw DE, White MA. 2022. The evolution of gene regulation on sex chromosomes. Trends
1015 Genet. 38(8): 844-855. doi: 10.1016/j.tig.2022.04.004
1016 Veitia RA, Potier MC. 2015. Gene dosage imbalances: Action, reaction, and models. Trends
1017 Biochem Sci. 40(6): 309-317. doi: 10.1016/j.tibs.2015.03.011
1018 Vicoso B, Bachtrog D. 2015. Numerous transitions of sex chromosomes in Diptera. PLoS Biol.
1019 13(4): e1002078. doi: 10.1371/journal.pbio.1002078

1020 Vicoso B, Emerson JJ, Zektser Y, Mahajan S, Bachtrog D. 2013a. Comparative sex chromosome
1021 genomics in snakes: Differentiation, evolutionary strata, and lack of global dosage
1022 compensation. PLoS Biol. 11(8). doi: 10.1371/journal.pbio.1001643
1023 Vicoso B, Kaiser VB, Bachtrog D. 2013b. Sex-biased gene expression at homomorphic sex
1024 chromosomes in emus and its implication for sex chromosome evolution. Proc Natl Acad
1025 Sci U S A. 110(16): 6453-6458. doi: 10.1073/pnas.1217027110
1026 Webster TH, et al. 2024. Lack of dosage balance and incomplete dosage compensation in the
1027 ZZ/ZW Gila Monster (*Heloderma suspectum*) revealed by de novo genome assembly.
1028 Genome Biol Evol. 16(3). doi: 10.1093/gbe/evae018
1029 Westfall AK, et al. 2021. A chromosome-level genome assembly for the Eastern Fence Lizard
1030 (*Sceloporus undulatus*), a reptile model for physiological and evolutionary ecology.
1031 Gigascience. 10(10). doi: 10.1093/gigascience/giab066
1032 Wright AE, Mank JE. 2012. Battle of the sexes: Conflict over dosage-sensitive genes and the
1033 origin of X chromosome inactivation. Proc Natl Acad Sci U S A. 109(14): 5144-5145.
1034 doi: 10.1073/pnas.1202905109
1035

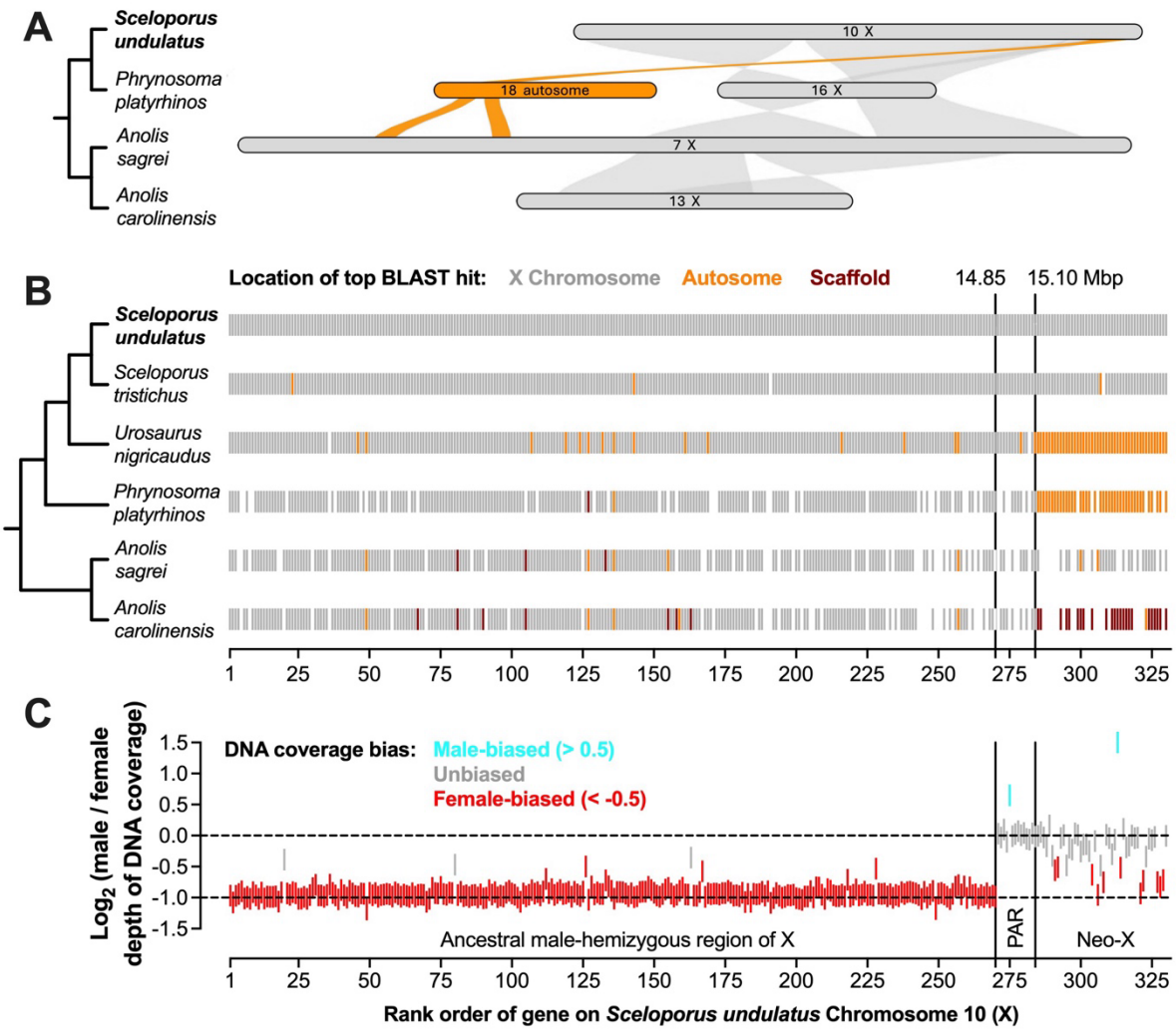

Figure 1. **(A)** Riparian plot illustrating synteny of *S. undulatus* chromosome 10 (X) with three other pleurodont genomes. Only chromosome-level scaffolds with syntenic blocks that map to *S. undulatus* chromosome 10 are shown. **(B)** Chromosomal locations of genes on *S. undulatus* chromosome 10 in five other pleurodont genomes, based on top BLAST hits using the longest mRNA isoform for each gene as a query. **(C)** Log_2 (male/female) depth of DNA sequencing coverage in *S. undulatus* for each gene on chromosome 10, with the dashed line at -1 signifying expected dosage imbalance due to hemizygosity in males. Vertical lines in **B** and **C** indicate inferred boundaries between the ancestral male-hemizygous region, ancestral psuedoautosomal region (PAR), and neo-X region in *S. undulatus* and *S. tristichus*.

1046 **Figure 2.**

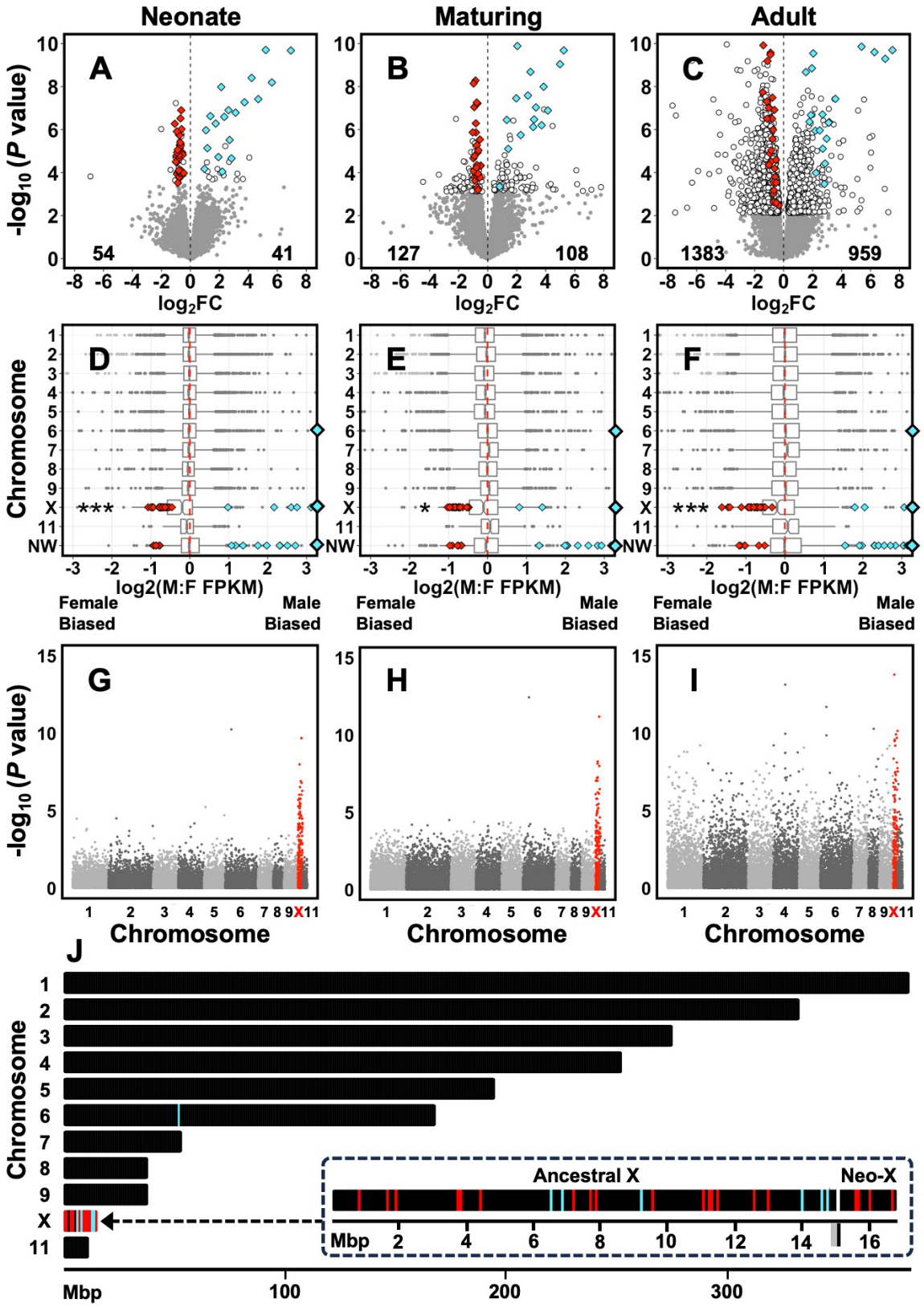

1047

1048 **Figure 2. (A-C)** Volcano plots depicting the magnitude ($\log_2$ fold change) and significance (-
1049 $\log_{10} P$ value) of sex-biased expression across 15,587 genes in liver of *S. undulatus* across three
1050 ages. Genes with significantly (FDR < 0.05) sex-biased expression (DEGs) are indicated in
1051 white, with the number of female-biased and male-biased DEGs indicated in the bottom corners
1052 of each panel. DEGs with consistently sex-biased expression across all ages are shown as red
1053 (female-biased) or blue (male-biased) diamonds. Grey points are genes that are not significantly
1054 sex-biased. **(D-F)** Boxplots depicting the median (line), interquartile range (box) and the smallest
1055 or largest values within 1.5 x IQR (whiskers) for sex-biased expression ($\log_2$ male:female ratio of
1056 fragments per kilobase per million mapped reads, FPKM) from each of the 11 largest scaffolds
1057 and pooled genes from unplaced scaffolds (NW) in the *S. undulatus* assembly. The 10th largest
1058 scaffold is the X chromosome. Notches in the center of each boxplot indicate the 95%
1059 confidence interval of the median. Diamonds indicate consistently female-biased (red) and male-
1060 biased (blue) DEGs in each tissue, which map predominantly to chromosome 10 (X) and
1061 unplaced scaffolds (NW). Diamonds on plot borders indicate DEGs beyond x-axis limits.
1062 Asterisks indicate when median chromosome expression deviates significantly from balanced
1063 male:female expression using Wilcoxon rank sum testing (mu = 0) with correction for multiple
1064 tests (* $P < 0.05$ without correction for multiple tests; ** $P < 0.017$, the critical alpha after
1065 Bonferroni correction; *** $P < 0.001$). **(G-I)** Manhattan plots of $-\log_{10} P$ values for sex-biased
1066 expression after ordering genes by chromosome and start position. All genes on X are shown in
1067 red. **(J)** Genomic locations of consistently sex-biased DEGs (unplaced scaffolds not shown).
1068 Enlarged inset shows that these genes occur on both the ancestral region of X that is hemizygous
1069 in males and on the putative neo-X region beyond the large tick mark at 15.1 Mbp. Gray shading
1070 immediately before this large tick indicates the putative psuedoautosomal region.

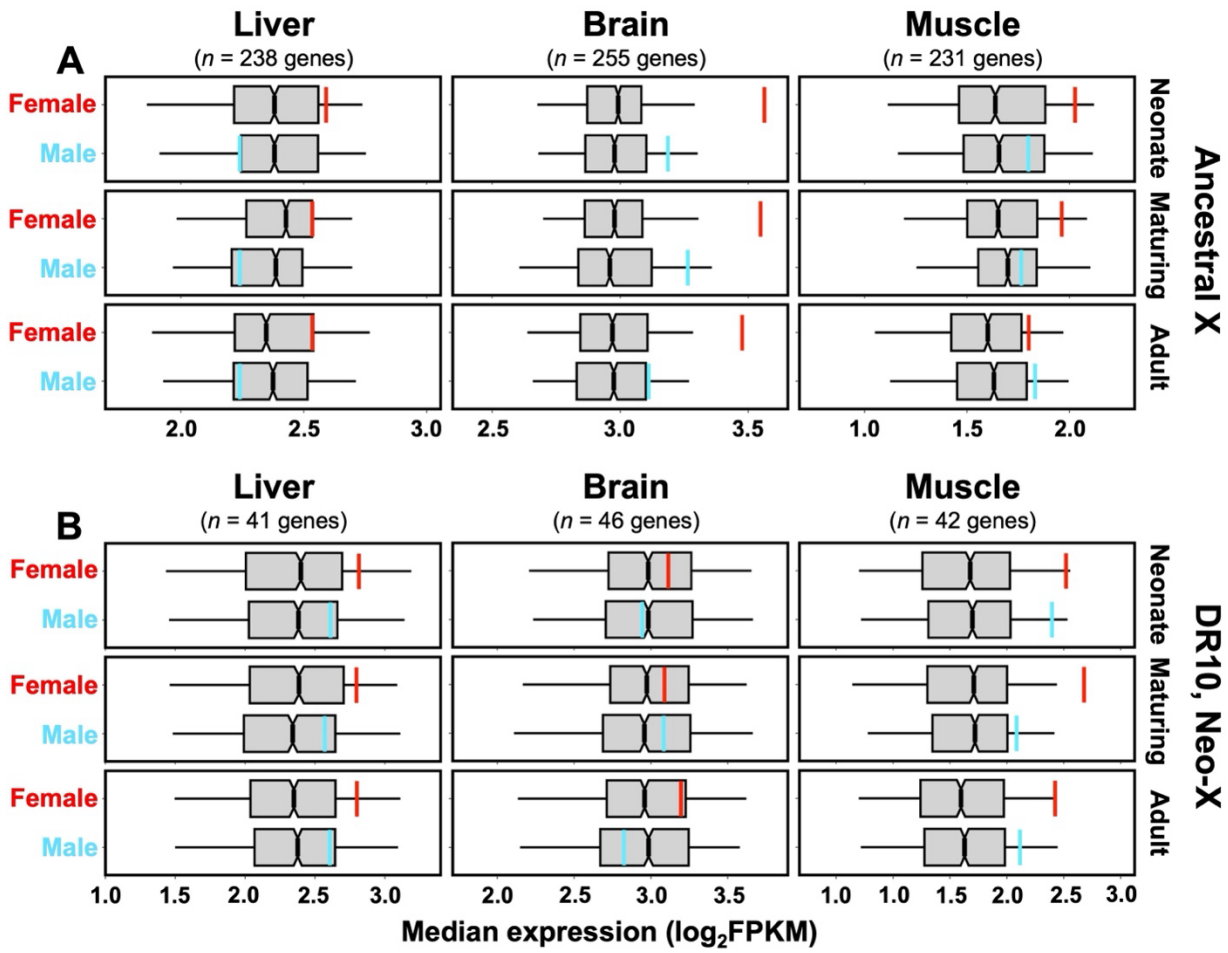

Figure 3. Comparisons of median expression on the X chromosome versus that of autosomes for each sex across three tissues and three ages in *S. undulatus*, shown separately for (**A**) the ancestrally X-linked 14.85-Mbp region of chromosome 10, and (**B**) the distal 1.76 Mbp region (DR10) that is more recently X-linked. Boxplots depict the median (line), IQR (box), and 5th and 95th quantiles (whiskers) for median expression estimates from 1000 randomly-sampled blocks of *n* contiguous autosomal genes (*n* = number of expressed genes in the corresponding region of the X chromosome in that tissue). Colored vertical lines (red = female; blue = male) indicate the median expression of all genes on X for each combination of sex, age, and tissue. Colored lines which fall beyond whiskers indicate that median expression of genes on the X chromosome differs significantly from the sampled distribution for autosomal genes.

1082 **Figure 4.**

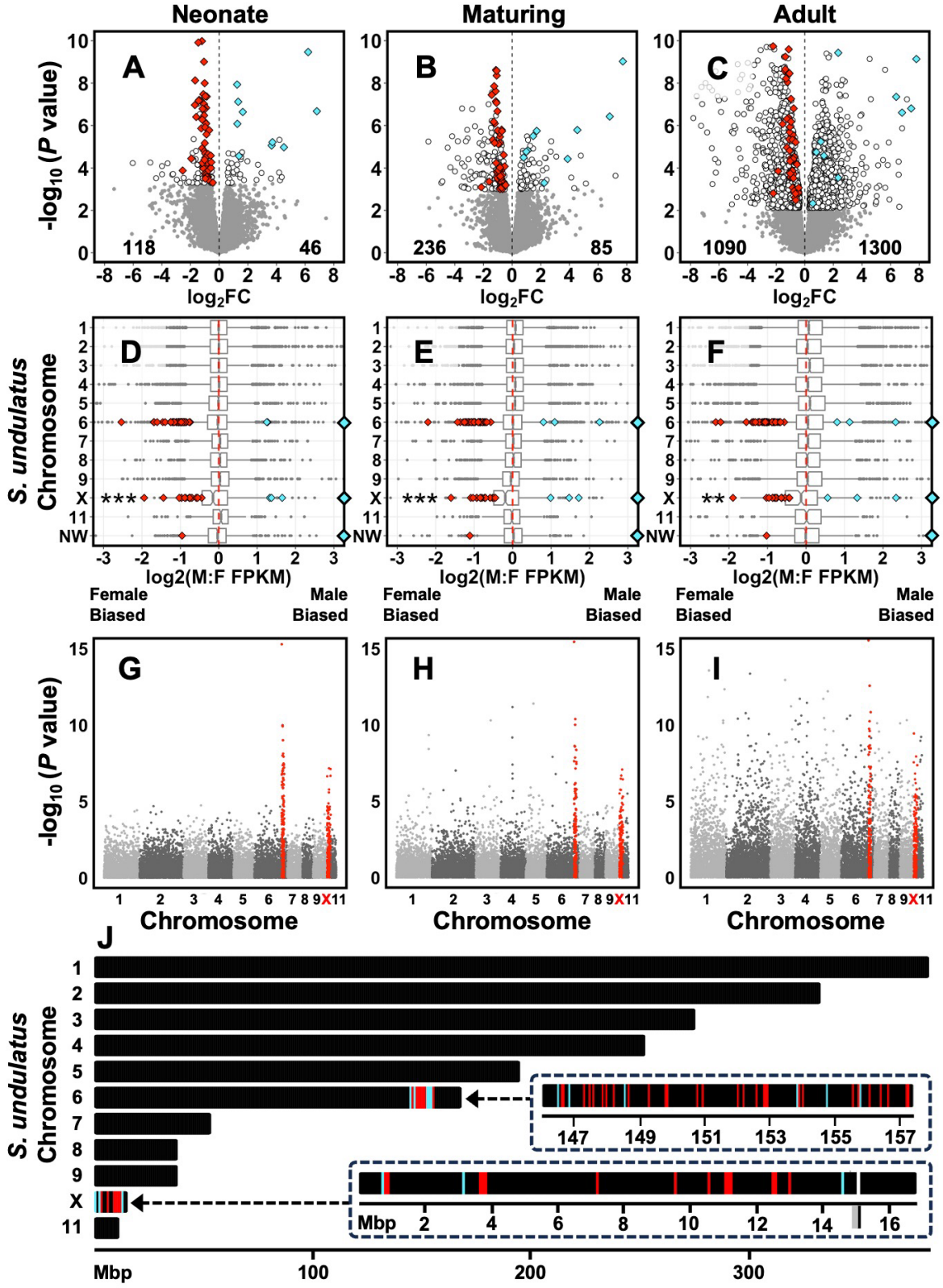

1083

1084 **Figure 4. (A-C)** Volcano plots depicting the magnitude (log_2 fold change) and significance (-
1085 log_{10} *P* value) of sex-biased expression across 15,493 genes in liver of *S. jarrovii.* Genes with
1086 significantly (FDR < 0.05) sex-biased expression (DEGs) are indicated in white, with the number
1087 of female-biased and male-biased DEGs indicated in the bottom corners of each panel. DEGs
1088 with consistently sex-biased expression across all ages are shown as red (female-biased) or blue
1089 (male-biased) diamonds. Grey points depict genes that are not significantly sex-biased. (**D-F**)
1090 Boxplots depicting the median (line), interquartile range (box) and the smallest or largest values
1091 within 1.5 x IQR (whiskers) for sex-biased expression (log_2 male:female ratio of fragments per
1092 kilobase per million mapped reads, FPKM) from each of the 11 largest scaffolds and pooled
1093 genes from unplaced scaffolds (NW) in the *S. undulatus* genome. Diamonds indicate consistently
1094 female-biased (red) and male-biased (blue) DEGs, which map predominantly to chromosome 6,
1095 chromosome 10 (X), and unplaced scaffolds (NW). Diamonds on plot borders indicate genes
1096 beyond x-axis limits. Asterisks indicate that median chromosome expression deviates
1097 significantly from balanced male:female expression using Wilcoxon rank sum testing (mu = 0)
1098 with correction for multiple tests (* $P < 0.05$ without correction for multiple tests; ** $P < 0.017$,
1099 the critical alpha after Bonferroni correction; *** $P < 0.001$). (**G-I**) Manhattan plots depicting -
1100 log_{10} *P* values for sex-biased expression after ordering genes by *S. undulatus* chromosome and
1101 start position. All genes on X and within an ~11 Mpb distal region of chromosome 6 (DR6) are
1102 shown in red. (**J**) Locations of consistently sex-biased DEGs in *S. jarrovii* when mapped to the *S.*
1103 *undulatus* genome. All consistently sex-biased DEGs map to the ancestral X chromosome (the
1104 region of *S. undulatus* chromosome 10 prior to the large tick at 15.1 Mbp in the lower inset) or
1105 the distal ~11 Mbp region of chromosome 6 (DR6, upper inset), suggesting that this region of *S.*
1106 *undulatus* chromosome 6 is X-linked in *S. jarrovii*.

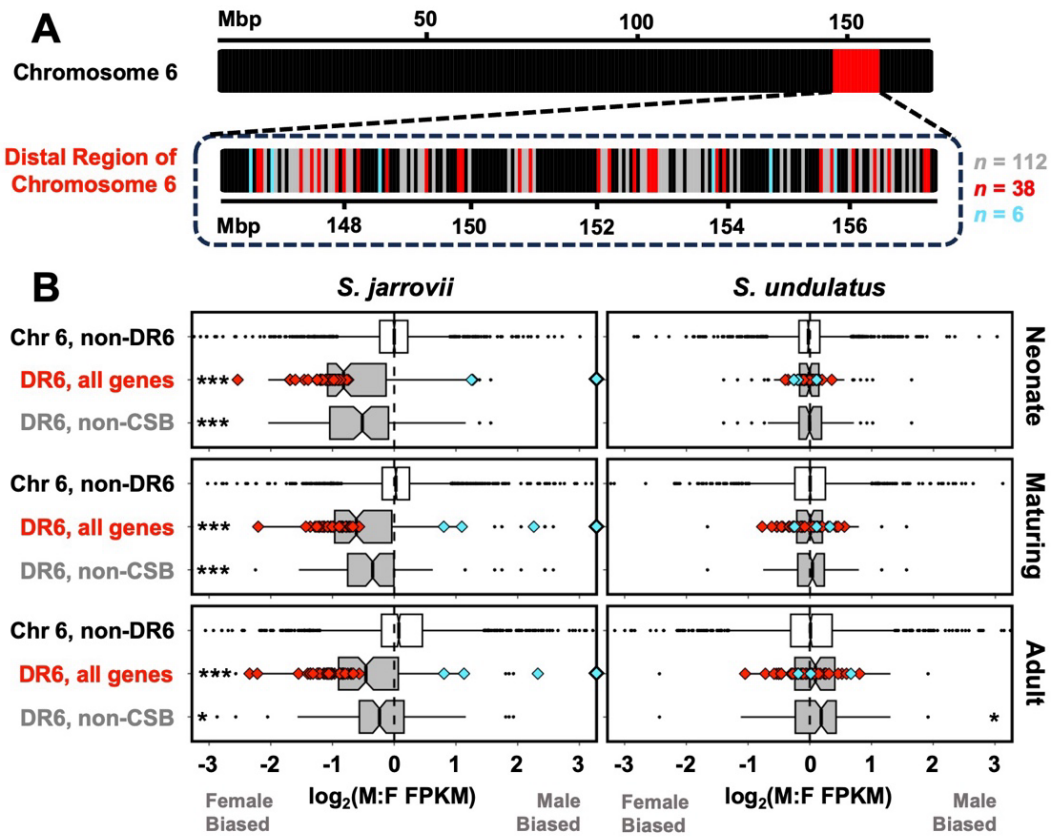

1107

1108 **Figure 5.** (**A**) Location of consistently female-biased (red), male-biased (blue), and unbiased
1109 genes (gray) in *S. jarrovii* that map to the distal region of chromosome 6 (DR6) in *S. undulatus.*
1110 Bars are not drawn to scale for gene length. (**B**) Boxplots depicting median (line), interquartile
1111 range (box), and 1.5 x IQR (whiskers) for sex-biased expression ($\log_2$ male:female ratio of
1112 fragments per kilobase per million mapped reads, FPKM) in liver of *S. jarrovii* and *S. undulatus*
1113 at three ages. Boxplots are show for all genes on chromosome 6 except those within DR6 ("Chr
1114 6, non-DR6"), for all genes within DR6 ("DR6, all genes"), and for all genes within DR6
1115 excluding consistently sex-biased DEGs ("DR6, non-CSB"). Diamonds depict consistently sex-
1116 biased DEGs with those on plot borders indicating sex bias beyond axis limits. Asterisks indicate
1117 when median expression differs from zero using Wilcoxon signed-rank tests with Bonferroni
1118 correction for 2 tests per age (* $0.025 > P > 0.001$; ** $0.001 > P > 0.0001$; *** $P < 0.0001$).

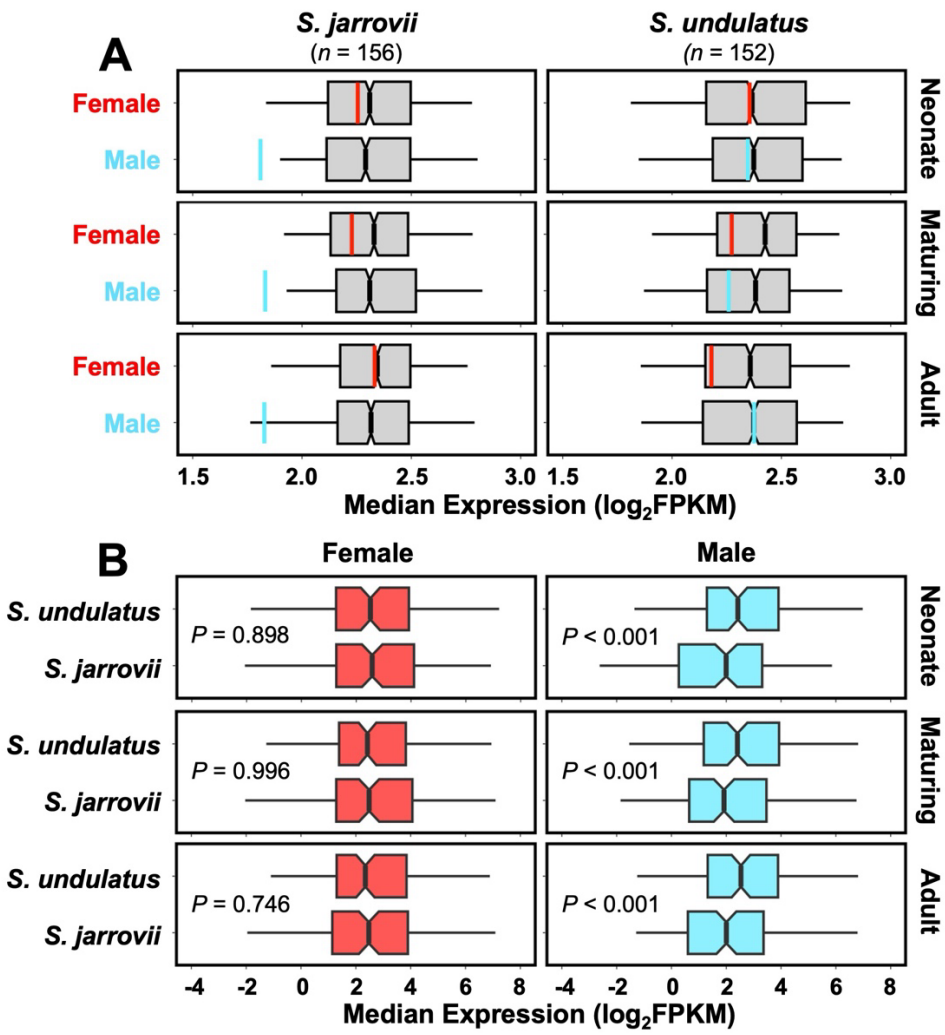

Figure 6. (**A**) Median expression of genes in the distal region of *S. undulatus* chromosome 6 (DR6) versus a sampled distribution of median autosomal expression for each sex across three ages in *S. jarrovii* and *S. undulatus*. Boxplots depict the median (line), intraquartile range (box), and 5th and 95th quantiles for median expression values from 1000 randomly sampled blocks of *n* contiguous autosomal genes (*n* = number of expressed genes within DR6 in each species). Vertical red (female) and blue (male) lines indicate median expression of all genes within DR6. (**B**) Comparisons (paired *t*-test by gene) of expression for all genes on DR6 between *S. jarrovii* and *S. undulatus,* conducted separately by sex. Boxplots depict median (line), intraquartile range (box), and 2.5th and 97.5th quantiles for expression of 152 genes present on DR6 in both species.

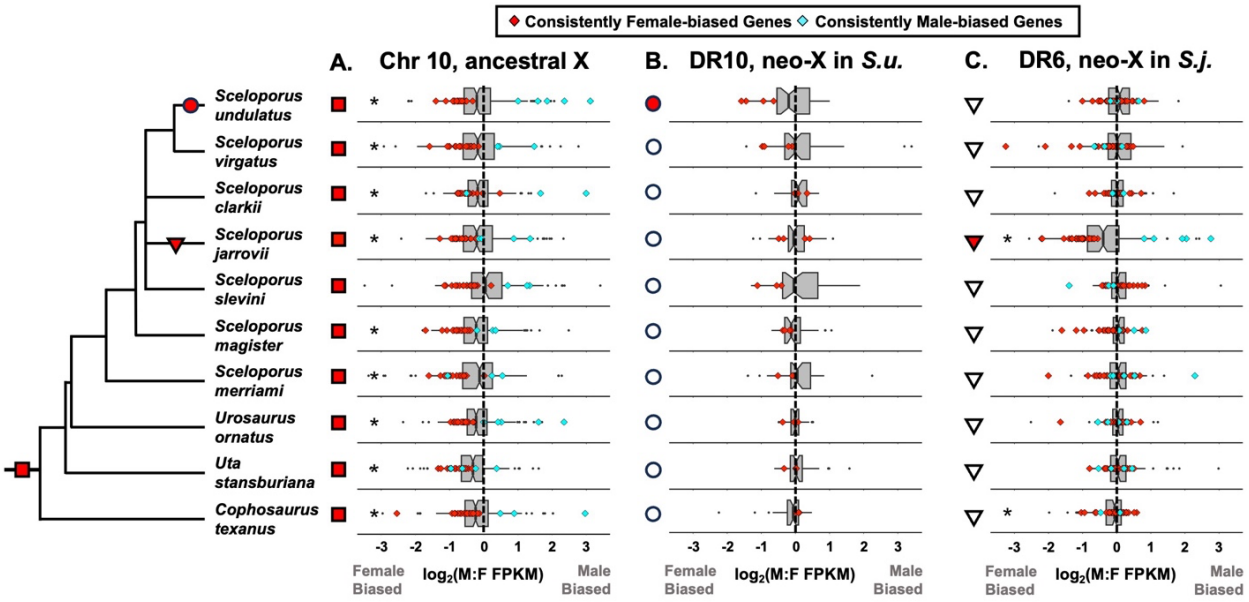

Figure 7. Evolutionary patterns in sex-biased expression of (**A**) the 14.85-Mbp region of *S. undulatus* chromosome 10 that is hemizygous in males (putative ancestral X), (**B**) the distal 1.76-Mbp region of chromosome 10 (DR10, putative neo-X region in *S. undulatus*), and (**C**) the distal 11-Mbp region of chromosome 6 (DR6, putative neo-X region in *S. jarrovii*) based on adult liver transcriptomes from 10 phrynosomatid species mapped to the *S. undulatus* assembly. Boxplots depict the median (line), intraquartile range (box), and 1.5 x IQR (whiskers) of $\log_2$ male:female expression (FPKM) for all expressed genes within each region. Diamonds indicate consistently female-biased (red) and male-biased (blue) genes in transcriptomes from *S. undulatus* (**A-B**) or *S. jarrovii* (**C**). Notches in boxplots indicate 95% confidence intervals of the median. Asterisks denote whether median expression ratios differ significantly from zero (Wilcoxon signed-rank test, Bonferroni-adjusted alpha = 0.005). Red symbols to the left of each boxplot indicate when consistently female-biased DEGs from *S. undulatus* (**A-B**) or *S. jarrovii* (**C**) differ from zero in each species (Wilcoxon signed-rank test, Bonferroni-adjusted alpha = 0.005) and are used to map ancestral (X) and derived (neo-X) male-female expression imbalances onto the phylogeny.